Link Adaptation for WiMAX Supported Mobile Hotspot

by

Md. Mahmud Hasan

A thesis
presented to the University of Waterloo
in fulfillment of the
thesis requirement for the degree of
Master of Applied Science
in
Electrical and Computer Engineering

Waterloo, Ontario, Canada, 2009

AUTHOR'S DECLARATION

I hereby declare that I am the sole author of this thesis. This is a true copy of the thesis, including any required final revisions, as accepted by my examiners.

I understand that my thesis may be made electronically available to the public.

ABSTRACT

In recent years, mobile hotspots have been getting much attention of the researchers. They are implemented on moving platforms. Research interests in mobile hotspots are motivated by the demand of seamless mobility. The IEEE 802.16e or mobile WiMAX opens a new door of possibility of mobile broadband. It provides extended mobility support and larger cell coverage. In this thesis we propose a simple link adaptation (LA) algorithm for the mobile hotspots, which are supported by (mobile) WiMAX network.

The role of link adaptation (LA) is very important because it controls the physical layer throughput. Therefore, all the higher layers are affected by LA. The main function of an LA algorithm is to select an appropriate burst profile. We consider downlink scenarios of WiMAX supported mobile hotspot. We formulate a discrete value optimization problem for LA, whose objective is throughput maximization. We choose forward error correction block rate (FBER) as constraint. The proposed LA algorithm comes as solution of the optimization problem. The proposed algorithm adapt with MAC layer performance. We develop a downlink channel estimation technique, propose an intra subchannel power allocation strategy, and propose an adaptive automatic repeat request (ARQ) mechanism as part of LA technique. We estimate SNR using channel estimation and intra subchannel power allocation. Then the estimated SNR is adjusted based on velocity of mobile hotspot. Adjusted SNR is used to select optimum burst profile.

The performances of the proposed LA algorithm are evaluated through numerical results obtained from link level simulations. According to numerical results, the proposed LA algorithm is able to maintain a certain level quality of service (QoS).

ACKNOWLEDGEMENTS

I would like to express my deepest gratitude to my supervisors, Professor Jon W. Mark and Professor Xuemin (Sherman) Shen for their priceless support and guidance towards this research. I would especially like to thank them for their patience and tolerance during my study period.

I would like to thank my sister Dr. Munira Sultana and my brother Md. Mahbub Hasan for their endless inspiration and support.

I would like to thank the Natural Sciences and Engineering Research Council (NSERC) of Canada for financial support under Grant No. RGPIN 7779.

I would like to thank my thesis readers, Professor Liang-Liang Xie and Professor Sagar Naik for reviewing this thesis. I am grateful to them for their valuable time in reviewing this thesis.

I would also like to thank my friends and colleagues in the broadband communication research (BBCR) group for their cooperation. I would like to offer my special thanks to Dr. M. Imadur Rahman of Ericsson, Tom H. Luan, Ahmed Barka, Suhail Al-Dharrab, Hangguan Shan, Yanfei Fan, Le Li, Hongtao Zhang, Feng Wang and Maazen Alsabaan for their help and assistance.

Dedicated

To my

Grandmother Kasiran

Contents

List of Tables

List of Figures

List of Acronyms

3G	Third generation cellular
4G	Fourth generation cellular
AAS	Adaptive antenna system
ACK	Acknowledgement
AMC	Adaptive modulation and coding
AP	Access point
ARQ	Automatic retransmission / repeat request
AWGN	Additive white Gaussian noise
BE	Best effort
BER	Bit error rate
BS	Base station
BPSK	Binary phase shift keying
CAMC	Combined AMC
CC	Convolutional coding
CDMA	Code division multiple access
CDF	Cumulative distribution function
CINR	Carrier-to-interference-and-noise ratio
CP	Cyclic prefix
CPS	Common part sublayer
CQICH	Channel quality indicator channel
CS	Convergence sublayer
CTC	Convolutional turbo coding
DL	Downlink
DTLA	Dynamic threshold link adaptation
ErtPS	Extended real time polling service
FBER	FEC block error rate

FBSS	Fast base station switching
FCH	Frame control header
FDD	Frequency division duplex
FEC	Forward error correction code
FIFTH	Fast Internet for the fast train host
FTP	File transfer ptotocol
FUSC	Fully used subchannelization
GSM	Global systems for mobile
HARQ	Hybrid ARQ
HHO	Hard handoff
ICI	Inter Carrier Interference
IEEE	Institute of electrical and electronic engineers
IETF	Internet engineering task force
IPP	Independent pilot pattern
ITU	International telecommunication union
LA	Link adaptation
LDPC	Low density parity check
LOS	Line of sight
LS	Least square
MAC	Medium access control (layer)
MAP	Medium access protocol
MCS	Modulation and coding scheme
MDHO	Macro diversity handover
MIMO	Multiple input multiple output
ML	Maximum likelihood
MN	Mobile node
M-QAM	M-ary QAM
MRC	Maximum ratio combining
MS	Mobile station
NACK	Negative Acknowledgement
NEMO	Network mobility

NLOS	Non line of sight
nrtPS	Non-real time polling service
OFDMA	Orthogonal frequency division multiple access
OFDM	Orthogonal frequency division multiplexing
PA	Power allcocation
PDU	Protocol data unit
PHY	Physical (layer)
PMF	Probability mass function
PMP	Point to multipoint
PUSC	Partially used subchannelization
QAM	Quadrature amplitude modulation
QoS	Quality of service
QPSK	Quarternary phase shift keying
RA	Resource allocation
RSSI	Received signal strength indicator
RTG	Receive transmit transition gap
rtPS	Real time polling service
SDU	Service data unit
SER	Symbol error rate
SF	Service flow
SISO	Single input single output
SOFDMA	Scalable Orthogonal frequency division multiple access
SM	Spatial multiplexing
SNR	Signal to noise ratio
STBC	Space time block code
TARQ	Truncated ARQ
TDD	Time division duplex
TTG	Transmit receive transition gap
UGS	Unsolicited grant service
UL	Uplink
VoIP	Voice over Internet protocol

WiMAX	Wireless interoperability for microwave access or World wide inter operation for microwave access
WLAN	Wireless local area network
WMAN	Wireless metropolitan area network
WWAN	Wireless wide area network
ZF	Zero Forcing

Chapter 1

Introduction

Supporting mobile hotspots over wireless networks is an emerging area of wireless communications. The term mobile hotspot refers to a hotspot, e.g., a wireless local area network (WLAN), located in a moving platform such as a vehicle. It provides Internet access to its terminals. In this thesis, we aim to develop a link adaptation (LA) algorithm for mobile hotspots, on the basis that the mobile hotspots will be supported by an IEEE 802.16e [1] WiMAX network. The most popular implementation of mobile hotspot is on a vehicle, in which the passengers can access the Internet using their terminal devices. These vehicles can be trains or buses. In general, there are two different network segments integrated together: the downward network segment is located inside the vehicle (mobile hotspot) and the network upward segment is located outside the vehicle. Therefore, a heterogeneous type of link plays a very important role. There is no unified system architecture for supporting mobile hotspots over the wireless networks. There are various types of system architectures devised for mobile hotspot implementation within a high velocity vehicle [2-8]. There are two major categories among these devised system architectures: satellite supported and mobile network supported. The satellite supported system was first developed under the fast Internet for the fast train host (FIFTH) project. The European Commission funded the FIFTH project to provide Internet facility within the high-velocity train. A Ku-band satellite plays the central role in this type of systems. In most of the cases the trains are directly connected through satellite links. In case of tunnel or underpass, where direct satellite links are not available, gap-filling networks are required. The gap-filling networks work as interface between mobile hotspot and satellite link. As the satellites cover a very large geographical area, the system does not experience any handoff oriented difficulties. This is the main advantage of this type of

mobile hotspot systems. The major drawbacks are the costs and unavailability of the satellites for public purpose.

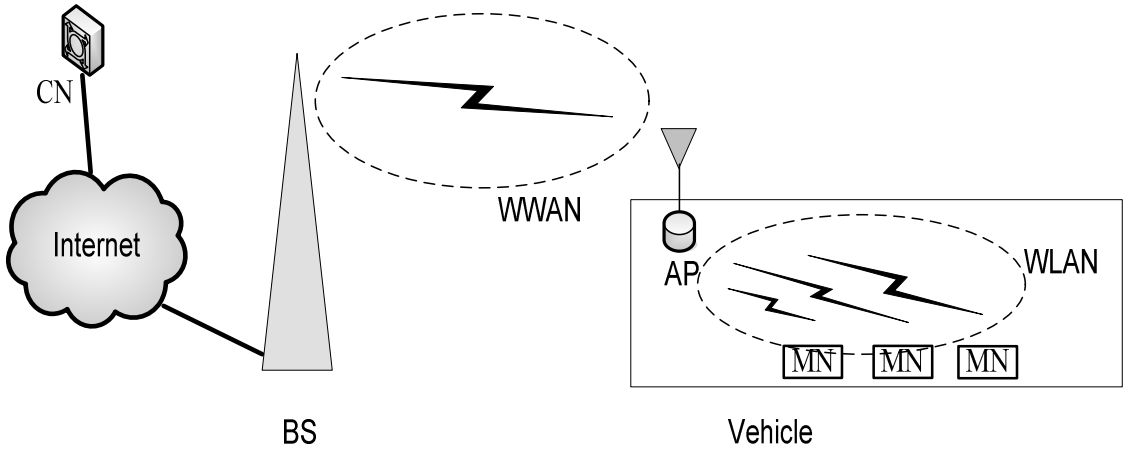

CN	Corresponding node
MN	Mobile node
AP	Access point
BS	Base station

Fig. 1.1 WWAN-WLAN based system architecture for mobile hotspot.

Although devised system architectures for the mobile network supported mobile hotspots are widely varied [2-4, 7-8], they have a common feature is that the downward network segments are the wireless local area networks (WLANs). WLANs are characterized by the different versions of IEEE 802.11 standards. The upward network segment can also be a satellite but it is not an essential part of this type of mobile hotspot systems. In this thesis, we devise a mobile network supported system architecture based on [2-3], which is the WWAN-WLAN based system architecture. The WWAN-WLAN based system architecture for mobile hotspot is shown in Fig. 1.1. In our system architecture, the upward network segment is a wireless wide area network (WWAN) based on IEEE 802.16e, and the downward network segment is a WLAN based on IEEE 802.11n standards. Integration of WWAN and WLAN provides larger service coverage for upward segment and larger user capacity for downward segment. More detailed on system architecture is provided in chapter 2.

1.1 Mobile WiMAX

Mobile WiMAX is a promising wireless access technology. It provides mobile broadband services. The present standard of mobile WiMAX is IEEE 802.16e. The terms "mobile WiMAX" and IEEE 802.16e are invariably used in the literature. The operation of mobile WiMAX is limited within the licensed band below 6 GHz. Therefore, it is free from the advantages (also disadvantages) of license exempt bands, and it is suitable for non line-of-sight (NLOS) mode of transmission. Mobile WiMAX supports mobile applications up to a vehicular speed of 120 km/hour. The gross data rate varies from 1 Mbps to 75 Mbps. It provides handoff facilities to the mobile stations. Recently, it has been commercially deployed in some areas in the world. Mobile WiMAX supports an all IP based network to overcome end-to-end bottleneck. These attractive features open a good market opportunity for mobile WiMAX. Hence, it is a strong competitor to the existing mobile communication systems (2.5 G, 3G, and 3G+). The IEEE 802.16 working group is now working on IEEE 802.16m (advanced air interface), which will support mobile applications with more advanced features such as higher throughput, more coverage, and higher mobility. It is expected that IEEE 802.16m will be the standard for future mobile WiMAX technology. Many countries around the world are working to build their own standards for 4G mobile communication systems. They are working individually and no unified approach for 4G network. No commercial deployment of 4G network is possible before 2010. Consideration of mobile WiMAX as a competitor to the future 4G technology is a very popular issue. At this moment, mobile WiMAX or IEEE 802.16e is one of the hottest areas of research.

1.1.1 PHY Overview

The PHY layer of IEEE 802.16e can be configured in either time division duplex (TDD) or frequency division duplex (FDD) mode. So far, it is optimized for the TDD mode only due to vendors' preferences. Most of the vendors prefer the TDD mode of the wireless MAN (WMAN) orthogonal frequency-division multiple access (OFDMA) PHY layer.

The frame structure consists of the downlink subframe and the uplink subframe. Two time gap intervals are used to separate these subframes. These gaps are known as transmit/receive transition gap (TTG) and receive/transmit transition gap (RTG). TTG and RTG allow the antenna to switch from transmit mode to receive mode and vice versa. TDD mode is analogous to TDMA technique where the same frequency band is shared by the different time slots (and also subframes). Each subframe is divided into some physical time slots to provide multiple user access. A scalable version of OFDMA (SOFDMA), which is capable to scale the number of subcarriers in a channel with possible values 128, 512, 1024 and 2048, is supported by 802.16e PHY layer [9-10]. We discuss more on OFDMA frame structure in section 2.2 of chapter 2. The allowed modulation schemes for UL and DL are: quarternary phase shift keying (QPSK), 16-quadrature amplitude modulation (QAM) and 64-QAM. The system can decide the proper modulation scheme and coding rate according to the current carrier-to-interference-and-noise ratio (CINR) value. The CINR of an MS varies with time. The base station (BS) determines the appropriate burst profile for each downlink and uplink data burst. The IEEE 802.16e PHY is also capable of supporting smart antenna or multiple-input-multiple-output (MIMO) systems and adaptive antenna system (AAS). MIMO and AAS are used to improve coverage and capacity. Various types of advanced technologies like beamforming, space time block code, spatial multiplexing are applied in MIMO systems. Among the other advanced PHY layer features, hybrid automatic repeat request (HARQ) and fast channel feedback (CQICH) are quotable. A channel quality indicator (CQI) is utilized to provide channel state information from the user terminals to the base station scheduler. Relevant channel state information can be fed back by the CQICH including: physical CINR, effective CINR, MIMO mode selection and frequency selective subchannel selection. We put special attention on subchannelization in subsection 2.2.2 of chapter 2.

A dedicated ACK channel is also provided in the uplink for HARQ ACK/NACK signaling. Multi-channel HARQ operation is also supported by mobile WiMAX. HARQ is enabled using N channel “stop and wait” protocol which provides fast response to packet errors and improves cell edge coverage. Chase combining and incremental

redundancy are two HARQ modes supported to further improve the reliability of the transmission. In the chase combining mode, the bit puncturing pattern of the retransmitted frames is kept the same as the first transmitted frame. All the retransmitted frames are combined with the first transmitted frame for error correction. In incremental redundancy mode, the number of channel coding bits is increased in every retransmission. Thus error correction capability is increased in every retransmission.

1.1.2 MAC Overview

The IEEE 802.16 system was developed to deliver broadband services such as voice, data and video [1], [9], [12]. The MAC layer of IEEE 802.16e supports a point-to-multipoint (PMP) architecture. The MAC scheduler allocates time slots among the mobile stations (MSs). The size of allocation to a single MS varies from a single time slot to the entire frame. A large dynamic range of throughput can be observed for an MS at any given time. The resource allocation information is conveyed in the MAP messages at the beginning of each frame. The scheduler is able to perform frame-by-frame adaptive scheduling based on the traffic characteristic. Prior to provide a certain type of data service, the base station (BS) and MS first establish a unidirectional logical link connection between the peer MACs. A connection is only for one type of service, i.e., different type of services can not be on the same MAC connection. The service flow (SF) defines the QoS service parameters for the packets or protocol data units (PDUs) that are exchanged on the connection. Mobile WiMAX can meet the QoS requirements for a wide range of data services and applications. These services and applications are summarized in Table 1 [9]. All services are connection oriented.

The MAC layer consists of three sublayers: convergence sublayer (CS), common part sublayer (CPS) and security sublayer. The CS handles a mapping from different types of transport layer traffic to the MAC formatted connections. Each service, including the connectionless service, is mapped to at least one connection. The CS classifies the service data units (SDUs) to a proper connection with specific QoS parameters. The CPS controls fragmentation, packing, scheduling, retransmissions, etc. The security sublayer provides

subscribers with privacy, authentication, or confidentiality across the broadband wireless network.

Table 1.1: Mobile WiMAX applications and QoS specifications.

QoS Category	**Applications**	**QoS Specifications**
UGS Unsolicited Grant Service	VoIP	Maximum sustained rate Maximum latency tolerance Jitter tolerance
rtPS Real-Time Polling Service	Streaming Audio and Video	Minimum reserved rate Maximum sustained rate Maximum latency tolerance Traffic priority
ErtPS Extended Real-Time Polling Service	Voice and Activity Detection (VoIP)	Minimum reserved rate Minimum sustained rate Maximum latency tolerance Jitter tolerance Traffic priority
nrtPS Non- Real-Time Polling Service	File Transfer Protocol (FTP)	Minimum reserved rate Maximum sustained rate Traffic priority
BE Best-Effort Service	Data Transfer, Web Browsing etc.	Maximum sustained rate Traffic priority

Mobility management functions are also supported by the MAC. Battery life time and handoff are two critical issues for mobile applications. These include power management and handoff. Mobile WiMAX supports sleep mode and idle mode for power efficient operation. Sleep mode is a state in which the MS conducts pre-negotiated periods of absence from the serving base station air interface. These periods are characterized by the

unavailability of the MS, as observed from the serving base station, to downlink or uplink traffic. The sleep mode also provides flexibility for the MS to scan other base stations to collect information to assist handoff during the sleep mode. Idle mode provides a mechanism for the MS to become periodically available for downlink broadcast traffic messaging without registration at a base station as the MS travels in an area populated by multiple base stations. It removes the necessity of frequent handoff. There are three handoff methods supported by the mobile WiMAX, hard handoff (HHO), fast base station switching (FBSS) and macro diversity handover (MDHO). The HHO is a mandatory feature of mobile WiMAX. In the FBSS, the MS and BS maintain a list of BSs that are involved in FBSS with the MS. This list is called an active set. The MS continuously monitors the BSs in the active set. Among the BSs in the active set, an anchor BS is defined. When operating in FBSS, the MS only communicates with the anchor BS for uplink and downlink messages including management and traffic connections. Transition from one anchor BS to another is performed without invocation of explicit signalling messages. In the MDHO, the MS and BS maintain an active set of BSs that are involved in MDHO with the MS. An anchor BS is defined among the active set. When operating in MDHO, the MS communicates with all BSs in the active set of uplink and downlink unicast messages and traffic. An MDHO begins when an MS decides to transmit and receive unicast messages and traffic from multiple BSs in the same time interval. It is able to provide diversity in both downlink and uplink.

1.2 Mobile Hotspot

The concept of mobile hotspot comes from the concept of network mobility (NEMO). The Internet engineering task force (IETF) governs the NEMO working group, which defines the basic protocol standards for seamless Internet connectivity to the mobile platforms [11]. This basic protocol supports the network layer. In order to make the feasible implementations of such systems researchers are paying attentions to the PHY and MAC layers. The NEMO includes aircrafts, ships, high-speed vehicles, etc. Many researches have been conducted under the term NEMO. In fact this is a huge area of research with numerous directions.

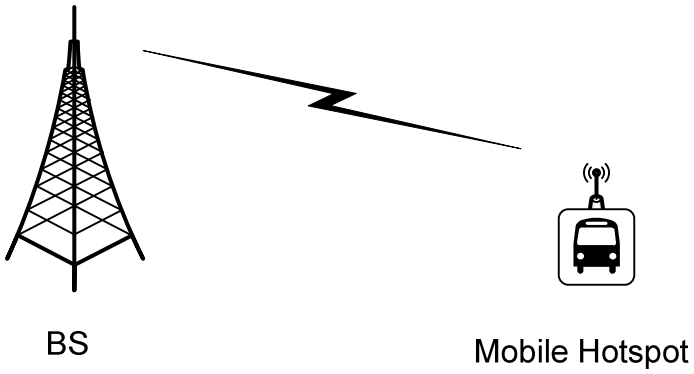

Fig. 1.2 A public transport mobile hotspot.

The terminology of 'mobile hotspot' is relatively new. In our thesis, we are going to emphasize on the mobile hotspots which are implemented on the high-speed vehicles like bus and train, i.e., the public transportation systems. Fig. 1.2 shows a typical scenario of a public transport mobile hotspot. This type of mobile platform is devised to meet the demand of seamless mobility. The main purpose of mobile hotspots is to provide Internet access within moving vehicles so that its passengers get connected.

1.3 Research Motivation

In the literature, WiMAX is often deemed as the service providing technology for the mobile hotspots. This comes in the form of example of such a network which is capable of supporting the mobile hotspots through its wireless wide area network (WWAN). To the best of our knowledge, none of the published works on mobile hotspots entirely considers WiMAX scenarios in their simulations or emulations. This happens because most of the published works deal with higher layer issues of the mobile hotspots. Only PHY and MAC layers are specified in the standard for mobile WiMAX (IEEE 802.16e). The mobile hotspots are implemented on the high velocity vehicles. Therefore, we consider WiMAX as an appropriate wireless access technology, which has larger area coverage and mobility support for the high velocity vehicles.

As the vehicles (mobile hotspots) move with high velocity, the channel state does not remain the same at all. The propagation paths, attenuation factors, noise, fading effect, shadowing effect, and interference are changing with distance (time). The burst profiles must be adaptive with the channel state to gain expected level of performance. This situation reveals the necessity of link adaptation (LA) techniques for mobile hotspot. Only a good LA technique can maximize system throughput and maintain a satisfactory level of quality of service (QoS). The IEEE 802.16e is facilitated with adaptive modulation and coding (AMC) and multiple input multiple output (MIMO) based antenna systems. These techniques improve network capacity and reliability. MIMO can be implemented in many different ways. Adoption of MIMO features makes the design of LA techniques more challenging. Moreover, mobile WiMAX is a paradigm of OFDMA based system, where efficient spectrum usage is an everlasting research challenge. Here we will consider a downlink (from WiMAX base station to mobile hotspot's access point) scenario for mobile hotspots in WiMAX networks. We concentrate on physical layer aspects of LA. We formulate a discrete value optimization problem to solve the LA problem of the mobile hotspot. The problem is also concerned with the MAC layer error tracking.

1.4 Research Objective and Contributions

The main objective of this research is to develop an LA algorithm for WiMAX supported mobile hotspot. We consider a downlink scenario with single cell and single mobile hotspot. The main function of an LA is to select an appropriate burst profile that provides efficient spectrum utilization, while maintaining a satisfactory level of QoS. We choose normalized throughput as a measure of spectrum utilization and forward error correction block error rate (FBER) as a measure of QoS. In addition to these physical layer performance metrics, MAC layer performance is also taken into account. We consider ARQ messages as the indicator of MAC layer performance.

The Mobile WiMAX uses MIMO and OFDMA together. In OFDMA physical layer, a subchannel is the basic unit of bandwidth allocation. A group of subcarriers forms a subchannel. Subchannel allocation and inter subchannel power allocation are components of resource allocation (RA). We consider intra subchannel power allocation and burst profile selection as parts of LA formulation. The LA problem of each subchannel is independent. We solve the LA problem separately for each subchannel for each downlink subframe. We present the LA problem as a discrete value optimization problem. We propose an adaptive ARQ mechanism to reduce FBER. The problem is formulated in such a manner that the solution must deploy the proposed adaptive ARQ mechanism. In LA, the most important parameter is signal-to-noise ratio (SNR). We develop a channel estimation technique for the downlink of MIMO-OFDMA physical layer, and propose an intra subchannel power allocation strategy. Subcarriers in a subchannel will experience equal SNR under this power allocation strategy. Then SNR is estimated using channel estimation and the intra subchannel power allocation strategy. We construct the SNR threshold tables for each burst profile using channel response and FBER requirement.

Finally, we propose a simple LA algorithm. The LA algorithm adjusts estimated SNR based on the velocity of mobile hotspot. It selects MIMO transmission modes based on both spatial correlation and SNR. It assigns priorities to the burst profiles based on the channel factors, spectral efficiency, and ARQ message status. At last, the burst profile with the highest priority is selected. Performances of the proposed LA algorithm are evaluated through numerical results.

1.5 Thesis Outline

Chapter 1 (the current chapter) gives a brief overview of mobile WiMAX including some basic PHY and MAC layer features, then a brief introduction to the mobile hotspots, describes research motivation, and brief notes on research objective and contributions.

Chapter 2 presents system model, and problem formulation.

Chapter 3 describes SNR estimation procedure, power allocation strategy and the proposed LA solution for the WiMAX supported mobile hotspots.

Chapter 4 provides some numerical results to evaluate the performance of the proposed LA algorithm.

Chapter 5 gives a brief conclusion and the suggestions for future work.

Chapter 2

System Model and Problem Formulation

In this chapter, we present the detailed system description including system architecture, physical layer, MAC layer error control and system model. We then address the throughput maximization problem to be solved using an LA algorithm.

2.1 System Architecture

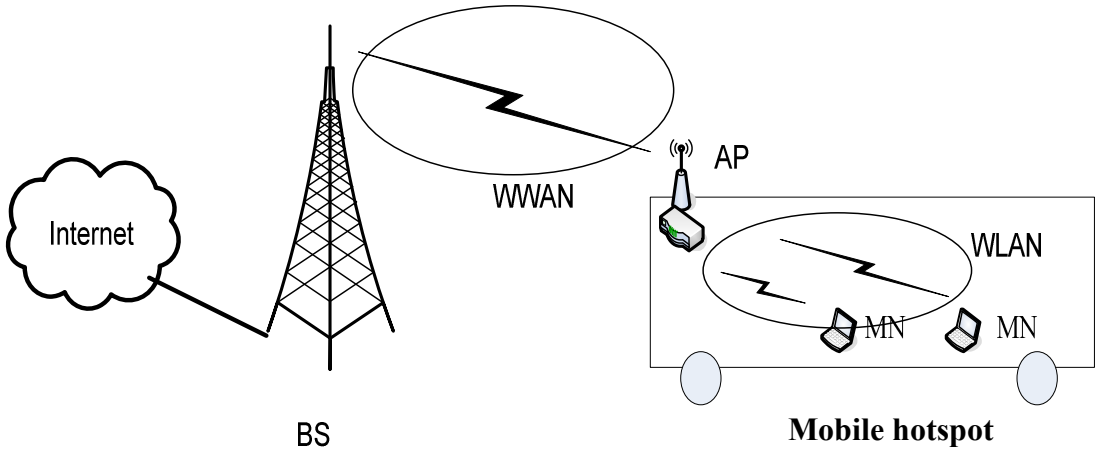

Fig. 2.1 System architecture for the WiMAX supported mobile hotspots.

We consider a single cell, single user (only one mobile hotspot) scenario. The base station (BS) is situated at the centre of the cell. An omni directional antenna system is mounted on top of the BS. This BS is an entity of cellular mobile WiMAX network. The BS is connected with internet through a wire line or an optical fiber link. The access point (AP) is mounted within the mobile hotspot. The mobile hotspot can be a public transport,

which moves with high velocity. Mobile WiMAX offers larger cell sizes with respect to the traditional mobile communication systems. This feature reduces handoff rate significantly. The AP communicates with the BS through the roof top antenna system. It acts as a mobile router or gateway for the downward network, i.e., the WLAN within the mobile hotspot. The AP is just an interface between two types of network. It has two separate antenna systems to communicate with each type of network segment. All the mobile nodes (MNs) within the vehicle are connected with the AP through the IEEE 802.11n based WLAN. These MNs can be laptops or other handheld devices, which are carried by the passengers. We will not talk much about the WLAN or the downward network segment; our focus will be restricted within the WiMAX based network segment. The system architecture is shown in Fig. 2.1. The main purpose of mobile hotspot is to provide internet access so that its passengers get connected. As most of the application requires downloading from the internet, the downlink traffic load is much higher than the uplink traffic. The downlink traffic route has two parts: the first part is situated between the BS and the AP, the second part is situated between the AP and the MNs. The downlink portion between the BS and the AP is the link of our interest. The AP receives information packets from the BS and stores them in a buffer for further processing. The MNs expose very limited mobility within the mobile hotspots. On the other hand, high mobility is exposed by the APs (mobile hotspots). The role of BS-AP link is more critical than that of AP-MN link. This is because the BS-AP link experiences a highly dynamic channel behavior. Fortunately, the network entity of the BS-AP link is powerful in terms of computational power and battery power. Unlike the traditional mobile systems like GSM and CDMA, the BS of mobile WiMAX is capable of processing complicated tasks. The entire mobile hotspot itself is a mobile station (MS). The APs are much more powerful compared to the ordinary MSs. Moreover, the physical dimensions of the APs are suitable for the MIMO based antenna systems. The MIMO based antenna systems improve data rate and reliability. In a MIMO system, there are multiple channels formed due to antenna diversity, one channel per transmit-receive antenna pair. It is required to keep these channels uncorrelated to each other. In practice, it is almost impossible to keep them totally uncorrelated. Correlations mainly depend on antenna element separation distance. It is required at least one wavelength, λ, (13 cm for 2.3 GHz) separation to

achieve significant diversity. But good performance is achieved between 10λ to 20λ separation [12]. The WiMAX BSs can provide 20λ antenna separation. The APs of the mobile hotspots can provide at least 15λ (6.5 ft.) separation for a 2×2 MIMO system. A MIMO system can be operated either in space time block code (STBC) mode or in spatial multiplexing (SM) mode. The STBC mode improves transmission reliability by using diversity. On the other hand, the SM mode improves transmission data rate by using multiplexing. In our system, we are considering a 2×2 MIMO system which can switch between these two modes based on channel condition. This type of MIMO system was first proposed in [13]. Though the higher order MIMO systems are more beneficial, they increase system complexity.

Any vehicle has a velometer to measure its velocity; our mobile hotspot is also equipped with a velometer to measure its velocity accurately. This is another good feature of the mobile hotspots, whereas the ordinary MS or MN could not measure its velocity. This information has a very important use in our signal-to-noise ratio estimation, which will be described in the next chapter.

2.2 Physical Layer Description

In this section, we describe the physical layer of the WiMAX supported mobile hotspots. Our discussions will focus on the following four features: subchannelization, OFDMA frame structure, forward error correction code (FEC) block structure and MIMO antenna systems. Our LA algorithm is highly dependent on these physical layer specifications. The mobile WiMAX physical layer supports both time division duplex (TDD) and frequency division duplex (FDD). In case of a mobile hotspot, passengers are mostly interested in downloading. Specially, the multimedia services are attractive to them. It requires higher bandwidth for the downlink. As FDD does not support asymmetry between uplink and downlink traffic, TDD is preferable. We have chosen the TDD mode of operation with a 3:1 downlink to uplink ratio. Another important fact is the strategy for subchannelization, which is included within the OFDMA frame structure subsection. It also includes notes on some mandatory MAC messages.

2.2.1 Subchannelization

A subchannel is the basic unit of bandwidth allocation. It consists of a group of subcarriers. There are three types of subchannelization strategies in mobile WiMAX: (i) fully used subchannelization (FUSC), (ii) partially used subchannelization, and (iii) band adaptive modulation and coding (band AMC). In FUSC, the pilot subcarriers are assigned first; then the remaining subcarriers are pseudo randomly distributed among the subchannels. In PUSC, the available subcarriers are first pseudo randomly distributed among the subchannels, and then pilot subcarriers are assigned within each subchannel. In band AMC, only adjacent subcarriers can form a subchannel. An OFDMA frame may use one or more subchannelization strategies [14]. In case of high mobility, the PUSC performs the best among these strategies due to its frequency diversity [15]. Band AMC is the simplest subchannelization strategy; it performs the best for fixed or pedestrian mobility. We have chosen PUSC because we are considering a high mobility case. It is the best performing strategy for the high velocity scenario [15], due to its frequency diversity. In our case, we consider only PUSC. In downlink PUSC, the distribution of subcarriers takes two stages. In the first stage, adjacent subcarriers form physical clusters. Each cluster contains a total of 14 subcarriers, among them 2 pilot subcarriers and 12 data subcarriers. In the second stage, the physical clusters are mapped on the logical clusters by using outer permutation. Then logical clusters are mapped into six major groups. An inner permutation is applied on major groups to form subchannels. Each subchannel takes two clusters (total 28 subcarriers) from a major group, i.e., the member subcarriers of the same subchannel are the member of the same major group. There are 4 pilot subcarriers and 24 data subcarriers in a subchannel.

We consider the 2.3 GHz band of mobile WiMAX. The total bandwidth of our system is 10 MHz. It consists of 1024 subcarreiers with 10.94 KHz subcarrier spacing. The total number of subchannels is 30 for downlink.

2.2.2 OFDMA Frame Structure

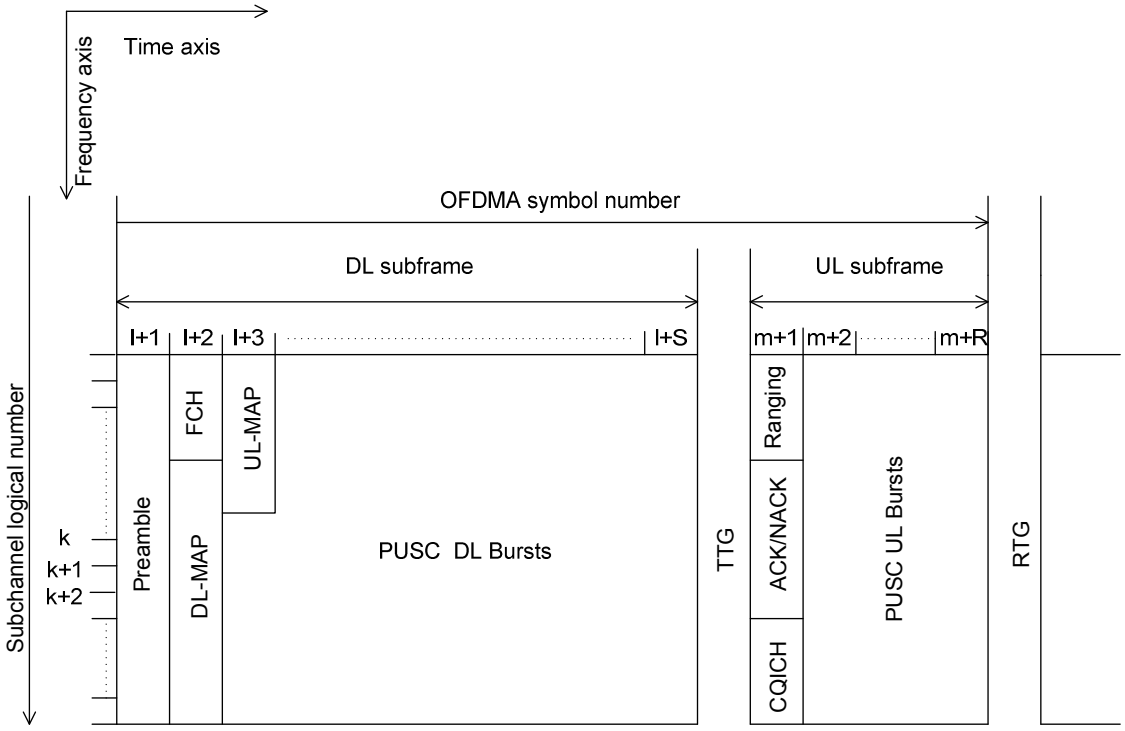

Fig. 2.2 OFDMA frame structure for TDD.

An OFDMA frame structure for TDD mode of operation is shown in Fig. 2. Though our focus is the physical layer, we include some mandatory MAC messages in this frame. The horizontal axis indicates the OFDMA symbol number (time domain), and the vertical axis indicates subchannel logical number (frequency domain). A time slot is the basic unit of allocation in the time domain. It consists of some OFDMA symbol duration. The content of a slot depends on the OFDMA symbol structure and the subchannelization strategy. In PUSC downlink a time slot consists of two symbol duration.

There are two main parts in the frame: downlink subframe and uplink subframe. Each frame begins with some mandatory control overhead: preamble, frame control header (FCH), downlink map (DL-MAP), uplink map (UL-MAP), transmit/receive transition gap (TTG) and receive/transmission transition gap (RTG). The preambles are used for

frame synchronization, channel state estimation, RSSI (received signal strength indicator) and CINR (carrier to interference and noise ratio) estimation. The FCH, DL-MAP, and UL-MAP describe the structure and composition of the frame. TTG and RTG takes place at the end of downlink and uplink subframes, respectively. A downlink burst indicates a rectangular allocation of a group of logically contiguous subchannels in a group of contiguous OFDMA symbols. A single modulation and coding scheme (MCS) is selected for each burst. This is signaled within the DL-MAP message and may include medium access control (MAC) protocol data units (PDUs) intended for one or more users. Each MAC PDU is segmented into FEC blocks. These blocks are coded and interleaved within a burst.

The first portion of uplink subframe consists of ranging information (Ranging), acknowledgement messages (ACK/NACK), and channel quality indicator (CQICH). The Ranging is used for synchronization and carrier tracking. The CQICH provides fast channel quality feedback. This information is used to construct the next downlink subframe. The roles of ACK/NACK and CQICH messages will play very important role in our LA algorithm. The automatic repeat request (ARQ) mechanism works based on ACK/NACK message. Since ARQ is a part of the MAC layer, we will discuss more on ARQ and hybrid ARQ (HARQ) in the next section. The BS is informed about channel quality through the CQICH message.

2.2.3 FEC Block Structure

We are paying special attention to FEC block because of the term FEC block error rate (FBER). FBER is widely accepted as a performance metric for mobile WiMAX [15], [16]. FBER appears in our problem formulation as a constraint to the throughput maximization. A burst is formed by a number of FEC blocks. An FEC block can be considered as the minimum allocation unit. The definition of FEC block can be varied from one system to another. Some early wireless systems defined it as a large information block which contains a number of packets. Sometimes, in WiMAX a whole burst is defined as an FEC block since the burst uses the same MCS for its subchannels. We

define it as the amount of information carried by one subchannel over one time slot. In case of PUSC subchannelization strategy, it is equivalent to 24 data subcarriers over 2 OFDMA symbol duration. Therefore, it consists of 48 modulation symbols. The size of an FEC block depends on MCS. In WiMAX, various types of channel coding are used: convolutional coding (CC), convolutional turbo coding (CTC), low density parity check (LDPC), etc. We consider only the CC for our downlink; CC is used as the inner code for the FEC blocks. The FEC block parameters are shown in Table 2.1. These MCSs with CC are supported by IEEE 802.16e downlink.

Table 2.1: Downlink FEC block parameters for CC.

Modulation Scheme	CC Coding Rate	Bits/symbol	Spectral Efficiency	FEC Block Size (bits)
QPSK	1/2	2	1	48
	3/4	2	1.5	72
16QAM	1/2	4	2	96
	3/4	4	3	144
64QAM	1/2	6	3	144
	2/3	6	4	192
	3/4	6	4.5	216

2.2.4 MIMO Antenna Systems

A noteworthy feature of mobile WiMAX is that it supports MIMO antenna systems. Our mobile hotspot will be connected with a mobile WiMAX network through an AP. We consider a MIMO antenna system which can switch between STBC and SM modes. According to the various research papers, STBC outperforms SM in the lower SNR scenarios and SM outperforms STBC in the higher SNR scenarios. That is why we want to exploit both modes by using a switching facility [13]. We consider a 2×2 MIMO

dimension for our downlink scenario. Two antenna elements are deployed in both of the network entities BS and AP. Figures 2.3(a) and 2.3(b) show the block diagrams of STBC and SM, respectively.

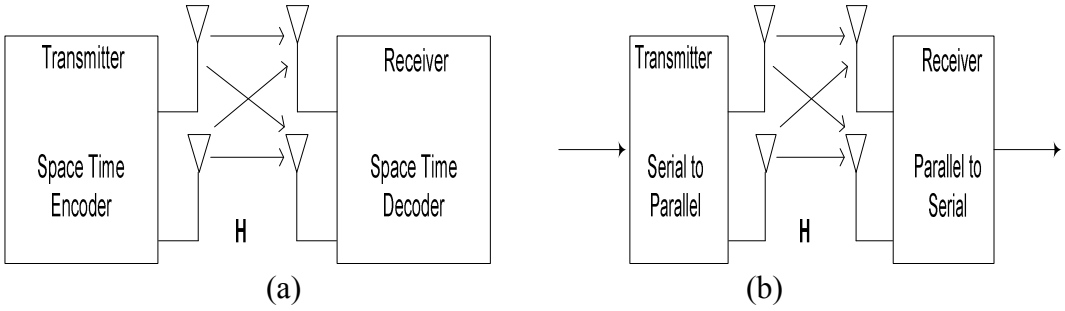

Fig. 2.3 MIMO systems (a) STBC, (b) Spatial multiplexing.

The basic idea of the STBC mode is to improve SNR by using space and time diversity. A coding technique plays the central role in achieving such diversity. The most widely used coding technique is the Alamouti STBC or the orthogonal STBC [17]. In our case, we consider Alamouti STBC with a maximum ratio combining (MRC) receiver. It takes two symbol durations to transmit two symbols. During the first symbol duration, two different symbols are transmitted simultaneously by using two different antennas. During the second symbol duration, two symbols are swapped with respect to their antennas and are transmitted again. Thus space and time diversity are achieved together. Since two symbols are transmitted during two symbol duration, the spectral efficiency remains the same for STBC. Improvement of SNR is the advantage from STBC, which ensures reliable transmission in a harsh environment.

The channel matrix of a $N_t \times N_r$ MIMO antenna system for subcarrier n is given by:

$$\mathbf{H}(n) = \begin{bmatrix} h_{11}(n) & \cdots & h_{1N_r}(n) \\ \cdots & \cdots & \cdots \\ h_{N_t 1}(n) & \cdots & h_{N_t N_r}(n) \end{bmatrix} \tag{2.1}$$

Each row element of the channel matrix corresponds to a transmitting antenna; each column element corresponds to a receiving antenna. Each element corresponds to a single input single output (SISO) channel response, i.e. the MIMO channel matrix is an array of SISO channel responses.

Let $s(n)$ denote the allocated power to subcarrier n for any symbol at the BS and σ^2 denote the variance of AWGN noise power at the mobile hotspot. Then we can write the post-detection SNR for Alamouti STBC mode with MRC reception as [15]:

$$\Gamma_{STBC}(n) = \frac{s(n)\sum_{i}^{N_t}\sum_{j}^{N_r}\left|h_{ij}(n)\right|^2}{\sigma^2 N_t} \tag{2.2a}$$

$$= \frac{s(n)\left\|\mathbf{H}(n)\right\|_F^{\,2}}{\sigma^2 N_t} \tag{2.2b}$$

where $\left\|\mathbf{H}(n)\right\|_F$ is the Frobenius norm of channel matrix $\mathbf{H}(n)$.

Let us consider the SM mode of MIMO antenna system. The main idea behind SM is to increase transmission rate by exploiting multiple antennas. There are two prerequisites for SM mode: SNR must be high and the MIMO channels are sufficiently uncorrelated to each other. At the transmitter side, a serial to parallel converter generates parallel bit streams as shown in the figure 2.3(b). These bit streams are transmitted by using different antennas, i.e., one transmitting antenna per bit stream. Since the bit streams are transmitted in parallel, the SM mode increases spectral efficiency. N_t independent bit streams (modulation symbols) are transmitted simultaneously at the same frequency. Unlike the STBC, there is no time diversity or space diversity. It has only the reception diversity at the receiver.

The optimum detection for SM mode is the maximum likelihood (ML) detection. ML detection requires an exhaustive search to find the fittest modulation symbol. This increases computational cost exponentially. Therefore, we consider the zero forcing (ZF) detector in our system for SM mode. Though it is not optimum, it is used for simplicity. The ZF detector is a linear detector, which sets a pseudoinverse of channel matrix $\mathbf{H}(n)$ to recover the transmitted information. The pseudoinverse of channel matrix is given by:

$$\mathbf{G}(n) = [\mathbf{H}(n)^{\mathbf{H}} \mathbf{H}(n)]^{-1} \mathbf{H}(n)^{\mathbf{H}} \tag{2.3}$$

where $\mathbf{H}(n)^{\mathbf{H}}$ is the Hermitian transpose of $\mathbf{H}(n)$. Let $s(n)$ denote the allocated power to subcarrier n for any symbol at the BS, and the symbol is transmitted by using the l^{th} transmitting antenna. The post-detection SNR for SM mode with ZF detector can be written as [15], [24]:

$$\Gamma_{SM,l}(n) = \frac{s(n)}{N_t \sigma^2 \left[\mathbf{G}(n)\mathbf{G}(n)^{\mathbf{H}} \right]_{ll}} \tag{2.4}$$

where $\mathbf{G}(n)^{\mathbf{H}}$ is the Hermitian transpose of $\mathbf{G}(n)$, and $\left[\mathbf{G}(n)\mathbf{G}(n)^{\mathbf{H}} \right]_{ll}$ is the (l,l) th element of the matrix $\mathbf{G}(n)\mathbf{G}(n)^{\mathbf{H}}$. $\left[\mathbf{G}(n)\mathbf{G}(n)^{\mathbf{H}} \right]_{ll}$ is also the square of Euclidean norm of the l^{th} row vector of $\mathbf{G}(n)$.

2.3 MAC Layer Error Control

In this section, we use the term frame to represent downlink subframe. MAC layer error control is done by an ARQ or HARQ mechanism. HARQ is supported in the physical layer of mobile WiMAX, but it is an optional feature. HARQ can be type I or type II. We propose an adaptive ARQ for our WiMAX supported mobile hotspot system, which uses a similar concept of combined and AMC-truncated ARQ (CAMC-TARQ) mechanism described in [18]. In a truncated ARQ mechanism, the transmitter waits for an ACK

message from the receiver. If there is no ACK or NACK message within a certain time interval, then the transmitter retransmits the same frame again. This routine continues up to certain number of retransmissions. If the frame is still erroneously received after that number, then the frame is dropped. In type I HARQ, all the transmissions are stored at the receiver and combined to get error free frames. The bit puncturing pattern is kept the same for all transmissions. This is also known as chase combining. If there exists any common erroneous portion among the retransmitted frames, chase combining can not avoid frame dropping. In that situation, there is no difference between the type I HARQ and the truncated ARQ. In type II HARQ, the bit puncturing pattern is changed in every retransmission due to the increment of redundant bits for channel coding. Both types of HARQ set a maximum limit for retransmission as the truncated ARQ. After that limit the frame is dropped. We observe that truncated ARQ and the HARQs do not use channel state information in the retransmissions. They require channel state information or the LA technique only at the first transmission. Another important fact is that, at least one retransmitted frame must be successfully received to avoid frame dropping.

In WiMAX, the whole MAC frame is logically partitioned into a number of smaller data blocks [19]. These data blocks are known as ARQ blocks. The size of an ARQ block is flexible, and varies from 1 to 2047 bytes. A single user may be connected with the BS through a single or multiple ARQ blocks. These blocks maintain the ACK/NACK channels independently. The main advantage of using smaller ARQ blocks is that, it prevents dropping of the whole MAC frame. An ARQ block is dropped after the maximum number of retransmissions. An ARQ block contains a number of FEC blocks. An FEC block is considered as erroneous when it contains at least one erroneous symbol and it is not correctable by FEC technique. On the other hand, an ARQ block is considered as erroneous block when it contains at least one erroneous FEC block. If the first transmission of an ARQ block is erroneous or failed then the retransmissions will occur. First time transmitted traffic is called non ARQ traffic and all the retransmitted traffic are called ARQ traffic. Non ARQ traffic and ARQ traffic can not coexist within the same ARQ block.

In our adaptive ARQ mechanism, channel state is required in every transmission and retransmission. The ARQ block structure can be modified or kept the same based on an LA technique. The main difference with truncated ARQ is that the block structure can be changed in every retransmission. After transmission of a downlink subframe, the BS will be waiting for the ACK/NACK messages from the mobile hotspot via uplink subframe. If an ARQ block is erroneous or its ACK/NACK message is not received by the BS, then the ARQ block structure will be revised and modified according to an LA technique. This routine will be continued up to a maximum number of retransmission. If the ARQ block still remains erroneous then it will drop the information carried by the first ARQ block only. This will also require at least one successful reception to avoid frame dropping. The similar concept of CAMC-TARQ mechanism can be applied in WiMAX. The combined CAMC-TARQ mechanism is also update the ARQ block structure in every transmission and retransmission based on SNR information. The results of [18] reveal the improvement of throughput using CAMC-TARQ mechanism. We add the impact of the previous erroneous reception with CAMC-TARQ concept to achieve higher level of adaptability. We consider erroneous reception as the sign of over estimation of SNR. Therefore, our LA algorithm will choose a burst profile with lower spectral efficiency in case of previous NACK. This impact is included in the LA problem formulation part. Therefore, an adaptive ARQ is embedded within our LA algorithm.

2.4 System Model

We model the downlink scenario between a BS and an AP of a mobile hotspot as shown in Fig. 2.4. The mobile WiMAX uses MIMO and OFDMA together; here we can use the term MIMO-OFDMA to describe our system. A MIMO-OFDMA transmitter is located at the BS and a MIMO-OFDMA receiver is located at the AP. The signals are transmitted through a multipath fading channel; we assume flat type Rayleigh fading and AWGN type noise. There exists an $N_t \times N_r$ MIMO antenna array between the transmitter and the receiver, where N_t and N_r are the numbers of antenna elements at the transmitter and the receiver, respectively. At the receiver, the information bits are extracted from the data

subcarriers and fed to the buffer. The pilot subcarriers are fed to the channel estimation block. This block estimates the channel responses for each subcarrier and records the current velocity of the vehicle (mobile hotspot) from the velometer. Then it sends this information to the BS by using the uplink subframe.

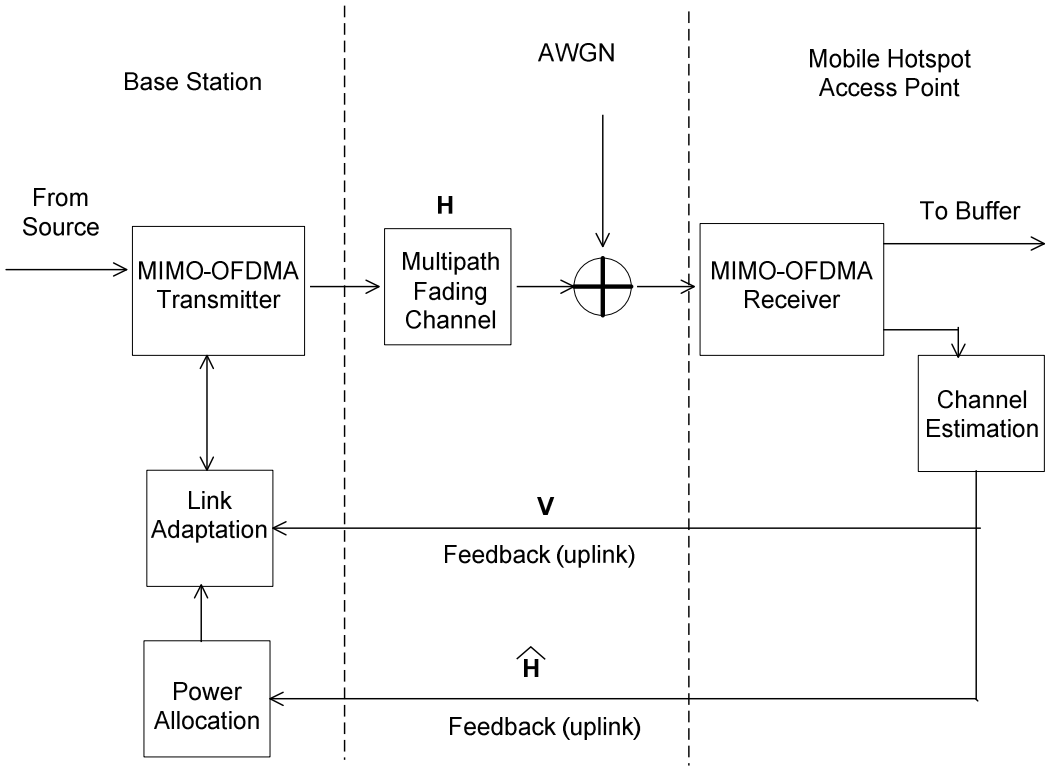

Fig. 2.4 Downlink system model.

A power allocation block works at the BS to allocate power among the subcarriers. It also computes the estimated post-detection SNR for each subcarrier. The link adaptation (LA) block selects the appropriate burst profiles for each subchannel. It gets the SNR values from the power allocation block. It also collects information on the ARQ blocks of the previous downlink subframe and current velocity. If an ARQ block in the previous downlink subframe is not acknowledged by the subsequent uplink subframe or negatively acknowledged (NACK), then retransmissions are performed up to a certain limit. ARQ is a part of the MAC layer; we did not show it on the figure. Our main interest is the LA

block, where our algorithm will work. The transmitter gets the decision on burst profile from the LA block.

2.4.1 FEC Block Error Rate and Throughput

There are three types of modulation used in mobile WiMAX: QPSK, 16-QAM and 64-QAM. We know that QPSK is equivalent to 4-QAM. Therefore, we can use the following equation to calculate symbol error rate (SER) of an M-QAM modulation [20]:

$$P_s = 4\left(1-\frac{1}{\sqrt{M}}\right)Q\left(\sqrt{\frac{3\Gamma_s}{M-1}}\right)\left[1+\left(1-\frac{1}{\sqrt{M}}\right)Q\left(\sqrt{\frac{3\Gamma_s}{M-1}}\right)\right] \tag{2.5}$$

Γ_s is the post-detection SNR per symbol, it may equal to Γ_{STBC} or $\Gamma_{SM,1}$ in our system. The relation between SNR per symbol and SNR per bit for M-QAM modulation with Gray-code can be given by [21]:

$$\Gamma_b \approx \frac{\Gamma_s}{\log_2 M} \tag{2.6}$$

The approximate expression for BER for M-QAM modulation with Gray-code and BER $\leq 10^{-3}$ is given by [22]:

$$P_b \approx 0.2\exp\left(\frac{-1.6\Gamma_b}{M-1}\right) \tag{2.7}$$

If the size of an FEC block is L_b bits, then the upper bound of FBER is given by:

$$FBER \leq 1-(1-P_b)^{L_b} \tag{2.8}$$

The expression (2.8) is true with equality when all bits are equally likely to be in error [15].

In a MIMO based antenna, the over all spectral efficiency depends on a factor named spatial coding rate. We denote spatial coding rate by μ. Spatial coding rate for a subcarrier is defined as the number of independent symbols transmitted per OFDMA symbol duration [23]. In our case,

$$\mu = \begin{cases} 1 & \text{for STBC} \\ N_t & \text{for SM} \end{cases} \tag{2.9}$$

Spectral efficiency of a burst profile with an M-ary modulation scheme, coding rate r, and spatial code rate μ, is given by:

$$\eta = \mu r \log_2 M \tag{2.10}$$

The normalized throughput for M-ary modulation with coding rate r and spectral efficiency η can be given by:

$$R = (1 - FBER)\eta \text{ bps/Hz} \tag{2.11}$$

2.5 Problem Description

The main function of LA technique is to select an optimal combination (burst profile) of MIMO transmission mode, modulation and coding scheme (MCS) based on channel state and QoS requirement. We use the term 'burst profile' to describe a combination of MCS and MIMO transmission mode. We do not consider inter subchannel power allocation as a part of LA. We leave it as a part of resource allocation. However, we discuss our strategy for intra subchannel power allocation in the next chapter. Our LA algorithm uses some necessary information: effective SNR per subchannel at the receiver end, FBER requirement, and ACK/NACK messages of ARQ blocks of the previous downlink

subframe. Our goal is to maximize throughput by means of this LA algorithm. The burst profile with higher spectral efficiency is deployed to achieve higher throughput. The corresponding burst profile must meet the system BER requirement. We set this BER correspond to a FBER. Ultimately, BER and FBER are both functions of SNR. There comes the importance of SNR information, the BS gets the channel response information from the AP. Most LA techniques define an SNR threshold level for each burst profile and compare with the current SNR, and then make a decision about the switching of burst profile. Unfortunately, exact SNR information is not available due to imperfectness of the estimation techniques and time varying nature of the wireless channels. Therefore, error tracking is required to make a proper selection of burst profile. We use NACK messages of the previous downlink subframe ARQ blocks as the warning signals in our LA algorithm. These signals are useful to select burst profile for the next downlink subframe. Another important factor is velocity; it is evident that the velocity of the vehicles (mobile hotspot in our case) has a significant impact on system throughput and packet error rate. From the literature, we know that if the packet transmission rate is higher than the Doppler frequency then the system throughput increases with higher velocity. If the packet transmission rate is lower than the Doppler frequency, then the system throughput decreases with higher velocity. In our deemed LA algorithm, we include the impact of velocity. We consider the impact of velocity in our SNR estimation procedures in the next chapter.

2.6 Problem Formulation

Our LA problem can be formulated as a discrete value optimization problem. We need to solve the same problem separately for each subchannel. This is due to the fact that different subchannel has different effective SNR. Roughly, effective SNR of a subchannel is the geometric mean of its member subcarriers' SNR. We formulate our LA problem to ensure efficient usage of spectrum with a satisfactory level of FBER. The dimension of one FEC block is one subchannel by two OFDMA symbol duration. Burst

profile for a subchannel will be selected for each downlink subframe. The generalized form of our optimization problem is as follows:

maximize $R_{i,k}(x)$

subject to $q_{i,k}(x) \le Q \qquad \forall i$

and $p_i(\eta_i, \rho) > 0 \qquad \forall i$

$i \in \{1, 2, 3.....,U\}$

$R_{i,k}(x)$ is the throughput for burst profile i, subchannel k, and effective SNR x. We set two preconditions for subchannel k: (i) it is allocated to the mobile hotspot, (ii) some power is allocated to subchannel k, and (iii) subchannel k does not carry information for more than one ARQ block for the same mobile hotspot (in the same downlink subframe). We also assume that the allocated power is sufficient to meet the SNR requirement of at least one burst profile. i is the burst profile index, and U is the number of possible burst profiles in our system. $q_{i,k}(x)$ is the FEC block error rate (FBER) for burst profile i, subchannel k, and effective SNR x. Q is the maximum tolerable FBER. $p_i(\eta_i, \rho)$ is the priority function for burst profile i. It is an additional constraint, which is introduced to adapt with erroneous reception of corresponding ARQ block in the previous downlink (DL) subframe. Priority function is a function of spectral efficiency (η_i), and erroneous reception indicator (ρ). We set this function to count the performance of the previous DL subframe. Higher values of this function indicate higher priorities and vice versa. It takes zero in case of the inappropriate burst profiles. We define priority function as:

$$p_i(\eta_i,\ \rho) = \eta_i I_{\{q_{i,k}(x)\le Q\}}[I_{\{i=\arg\max_j \eta_j I_{\{q_{j,k}(x)\le Q\}}\}} I_{\{\rho=0\}} + I_{\{i\neq\arg\max_j \eta_j I_{\{q_{j,k}(x)\le Q\}}\}} I_{\{\rho\ge 0\}}] \quad \text{for } \sum_i^U I_{\{q_{i,k}(x)\le Q\}} \ge 2 \tag{2.12a}$$

$$= \eta_i I_{\{q_{i,k}(x)\le Q\}} \quad \text{for } \sum_i^U I_{\{q_{i,k}(x)\le Q\}} = 1 \tag{2.12b}$$

where

η_i is the spectral efficiency of burst profile i;

$I_{\{\}}$ is the indicator function which takes the value either 1 or 0 depends on satisfaction of condition;

ρ takes the value 0 if the corresponding ARQ block in the previous downlink subframe was successfully received and 1 for erroneous reception;

$i, j \in \{1, 2, 3.....,U\}$ are the indices for the burst profiles.

The main reason behind introducing this function is that: if the corresponding ARQ block in the previous DL subframe is erroneously received, we may select the burst profile with the second highest spectral efficiency instead of the highest spectral efficiency. It will ensure more reliable transmission at the cost of spectral efficiency. It embeds an adaptive ARQ mechanism in our link adaptation algorithm.

Chapter 3

Link Adaptation for Mobile Hotspot

In this chapter, we describe SNR estimation procedure, intra subchannel power allocation strategy, SNR threshold table, and finally propose an LA algorithm for the WiMAX supported mobile hotspots. We use the term SNR to present SNR per symbol.

3.1 SNR Estimation

We have chosen pilot based channel estimation for our system. In mobile WiMAX, the pilot subcarriers are allocated for channel estimation. Our intention is to estimate channel response of each subcarrier at the mobile hotspot. Therefore, we will describe pilot based frequency domain channel estimation. At first, the channel response of each pilot subcarrier will be estimated by using a least square (LS) estimator. And then the channel response of the data subcarriers will be estimated by applying linear interpolation and linear extrapolation. We have selected this method because it reduces computational complexity. Moreover, an LS estimator requires comparatively less amount of prior knowledge. The main idea is "to estimate channel response of each pilot subcarriers then use it to estimate channel response of each data subcarriers". These channel responses are sent to the BS via the uplink. A power allocation (PA) unit is responsible for allocation power to these subcarriers at the BS. The LA unit is informed of the estimated SNRs after the power allocation is done.

Let us look at the subcarrier permutations in IEEE 802.16e based OFDMA systems. Since the partial usage of subcarriers (PUSC) provides the best performance for mobile

station (MS) with higher velocity [15], we prefer this subchannelization strategy. In downlink PUSC, all the subcarriers are divided into 60 clusters. Each cluster consists of 14 adjacent subcarriers. These clusters form six major groups. The subchannels are defined in the major groups. Two clusters are required to form a subchannel. These two clusters must be non adjacent but from the same major group. The positions of the pilot subcarriers are allocated by the subchannelization strategies. The positions of the pilot subcarriers for PUSC downlink are shown in Fig. 1. We see that pilot subcarriers are located based on the parity of OFDMA symbol. There are two pilot subcarriers allocated in each cluster. It means one cluster per OFDMA symbol. For the even OFDMA symbols, 5^{th} and 9^{th} subcarriers of each cluster are allocated as pilots. For the odd OFDMA symbols, 1^{st} and 13^{th} subcarriers of each cluster are allocated as pilots.

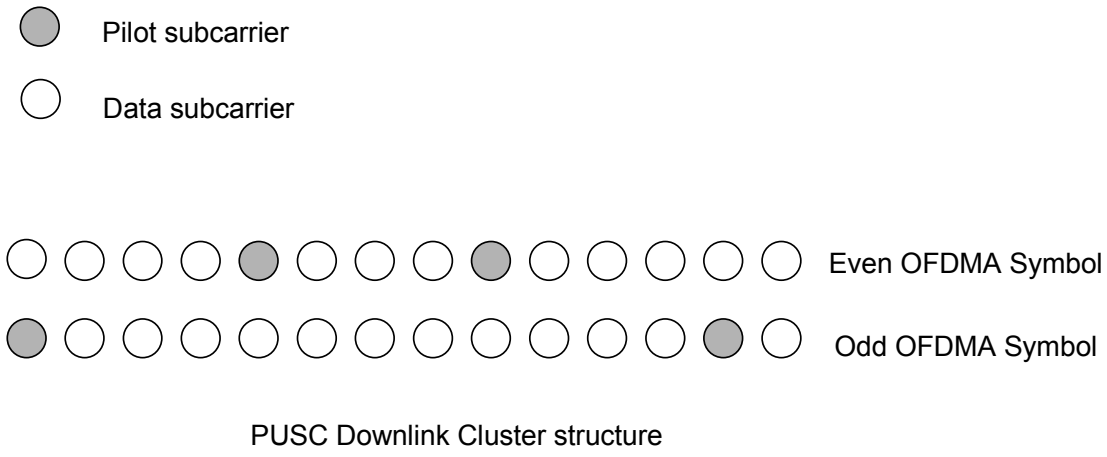

Fig. 3.1 PUSC downlink cluster structure.

3.1.1 Channel Response Estimation for the Pilot Subcarriers

The pilot subcarriers are known to the receiver. In other words, the receiver has some prior knowledge about the pilot subcarriers. Power level and modulation technique used for the pilot subcarriers are included as prior knowledge. An LS estimator estimates the channel response for each pilot subcarriers. In mobile WiMAX, the pilot subcarriers are BPSK modulated. The power allocated to each pilot subcarrier is a fixed value and it is known to the receiver.

At the beginning of channel response estimation, we restate some important facts about our system: we consider a single user downlink scenario where an AP of a mobile hotspot is the receiver, the transmitter is the BS. Our system is a 2×2 MIMO OFDMA system and capable of switching between STBC and SM transmission modes. In case of STBC, two transmitting antennas use different subcarriers at the same OFDMA symbol. In the next OFDMA symbol, they interchange their subcarriers. This is helpful for frequency domain channel estimation; the estimator can separate the channel response of each MIMO antenna pair. In case of SM, two antennas use the same subcarriers to exploit spatial multiplexing. The subcarriers are spatially multiplexed to achieve higher spectral efficiency. The pilot subcarriers do not require spatial multiplexing. If the same pilots are simultaneously transmitted by the two antennas, then it is difficult to separate the channel response of each MIMO antenna pair. Therefore, the pilot subcarriers are not spatially multiplexed. In other words, two antennas do not transmit the same pilot subcarriers simultaneously. This feature provides easier separation of channel responses of each MIMO antenna pair in the frequency domain. This approach of pilot based MIMO channel estimation is known as independent pilot pattern (IPP), [25].

Let us consider a transmitting-receiving antenna pair. We drop the antenna indices for convenience. In the frequency domain, the received pilot signal for a time varying multipath channel can be expressed as:

$$Y_{p,m}(f,t) = H_{p,m}(f,t)X_{p,m}(f) + W_{p,m}(f) \tag{3.1}$$

where p and m are the pilot and OFDMA symbol indices respectively.

$X_{p,m}(f)$ is the frequency domain presentation of the transmitted pilot signal.

$H_{p,m}(f,t)$ is the time varying transfer function of the channel.

$W_{p,m}(f)$ is the frequency domain presentation of the channel noise.

$H_{p,m}(f,t)$ is obtained from the Fourier transform of time varying impulse response of multipath channel [26]:

$$H_{p,m}(f,t) = F_{\tau}[h_{p,m}(\tau,t)] \tag{3.2}$$

or $H(f,t) = F_{\tau}[\sum_{l=0}^{L-1} h_l(t)\delta(\tau - \tau_l)]$ (we drop pilot and OFDMA symbol indices)

$$= \sum_{l=0}^{L-1} h_l(t)\exp(-j2\pi\tau_l f) \tag{3.3}$$

where $l \in \{0,1,2,.....L-1\}$ is the path index, delay is denoted by τ.

If the p[th] subcarrier is a pilot subcarrier, then the discrete version of the channel transfer function (for that pilot subcarrier) at the m[th] OFDMA symbol is given by [27]:

$$H_{p,m} = H_{p,m}(f = \frac{p}{NT}, t = mT_s) \tag{3.4}$$

$$= \mathbf{F_p h_m} \tag{3.5}$$

where N is the total number of subcarriers in our system, T is the sampling period, T_s is the symbol duration, and

$$\mathbf{F_p} = \left[\exp\left(-\frac{j2\pi p\tau_0}{NT}\right) \quad \exp\left(-\frac{j2\pi p\tau_1}{NT}\right) \quad ..... \quad \exp\left(-\frac{j2\pi p\tau_{L-1}}{NT}\right)\right] \tag{3.6}$$

$$\mathbf{h_m} = [h_0(mT_s) \;\; h_1(mT_s) \;\; ..... \;\; h_{L-1}(mT_s)]^T \tag{3.7}$$

In WiMAX, a cyclic prefix (CP) is added at the beginning of the OFDMA symbol. As a result, the over all symbol duration is longer than the data symbol duration. The CP allows the receiver to adapt with delay spread and to maintain frequency orthogonality [15], [19]. The time duration of CP is known as guard time. In mobile WiMAX, 1/8 is the mandatory ratio between guard time and data symbol duration. The symbol duration is given by,

$$T_s = (N + L_{CP})T \tag{3.8}$$

where L_{CP} is the length of CP in terms of number of samples per symbol duration. CP is also used for synchronization purpose. Hence, the discrete version of equation (3.1) can be written for the p[th] subcarrier at the m[th] OFDMA symbol as

$$Y_{p,m} = H_{p,m}X_{p,m} + W_{p,m} \tag{3.9}$$

$X_{p,m}$ is known to the receiver. The objective function of a least square (LS) estimator is

$\min \left\| Y_{p,m} - \hat{H}_{p,m}X_{p,m} \right\|^2$, which gives us the estimated channel response for the pilot subcarrier:

$$\hat{H}_{p,m} = \frac{Y_{p,m}}{X_{p,m}} = H_{p,m} + E_{p,m} \tag{3.10}$$

where $E_{p,m} = \frac{W_{p,m}}{X_{p,m}}$ is an error term due to channel noise and imperfectness of the LS estimator.

3.1.2 Channel Response Estimation for the Data Subcarriers

Channel responses for the data subcarriers can be estimated by using linear interpolation or linear extrapolation. The estimated channel response for any data subcarrier n (n is the physical index) at the m[th] OFDMA symbol is given by,

$$\hat{H}_{n,m} = \hat{H}_{p_A,m} + \frac{\hat{H}_{p_B,m} - \hat{H}_{p_A,m}}{p_B - p_A}(n - p_A) \tag{3.11}$$

where p_A and p_B are the pilot subcarrier physical indices and $p_B > p_A$. Also n, p_A and p_B are the members of the same cluster. Equation (3.10) performs linear interpolation where $p_A < n < p_B$. It performs linear extrapolation where $n < p_A$ or $n > p_B$.

We can apply the same technique for all the subcarriers and for all the OFDMA symbols. In case of odd OFDMA symbols, $h_{11}(n)$ and $h_{12}(n)$ can be estimated. In case of even OFDMA symbols $h_{21}(n)$ and $h_{22}(n)$ can be estimated. After that, the time average can be calculated for the entire downlink subframe. We use corresponding tiled version of symbols to denote estimated parameters, for example $\tilde{h}(n)$ is the estimated version of $h(n)$. In general we can write,

$$\tilde{h}(n) = \frac{2}{M}\sum_{m=1}^{M-1}\hat{H}_{n,m} \qquad \text{for odd symbols, } \tilde{h}(n) = \tilde{h}_{11}(n) \text{ or } \tilde{h}_{12}(n) \tag{3.12a}$$

$$\tilde{h}(n) = \frac{2}{M}\sum_{m=2}^{M}\hat{H}_{n,m} \qquad \text{for even symbols, } \tilde{h}(n) = \tilde{h}_{21}(n) \text{ or } \tilde{h}_{22}(n) \tag{3.12b}$$

where M is the total number of downlink symbols, which is always an even number. Hence, the estimated channel matrix $\tilde{\mathbf{H}}$ for each subcarrier is sent to the BS via uplink. The estimated average channel gain (spatial average) of a subcarrier n can be defined as,

$$\overline{\tilde{H}(n)} = \sqrt{\frac{1}{4}\sum_{i=1}^{2}\sum_{j=1}^{2}\left|\tilde{h}_{ij}(n)\right|^2}$$

$$= \frac{1}{2}\left\|\tilde{\mathbf{H}}(n)\right\|_{\mathbf{F}} \tag{3.13}$$

3.1.3 Estimated SNR and Power Allocation

In OFDMA, we may separate weak subchannels from the strong subchannels. But we do not have that option at the subcarrier level. SNR is highly dependent on power allocation strategy. We need to allocate sufficient power to the member subcarriers of a subchannel so that they meet the SNR requirements for a particular symbol error rate (SER). We left inter subchannel power allocation for the resource allocation (RA). Our LA algorithm will select burst profile for each subchannel. This decision will be made based on the estimated effective SNR. Here we describe an intra subchannel power allocation strategy.

Let $\overline{\tilde{H}_k(n)}$ be the estimated average channel response of the nth subcarrier of the kth subchannel, and $s_k(n)$ be the allocated power to that subcarrier. Then the estimated SNR at the receiver end is given by,

$$\tilde{\Gamma}_k(n) = \frac{s_k(n)\left|\overline{\tilde{H}_k(n)}\right|^2}{\sigma^2} \tag{3.14}$$

The estimated effective SNR of the kth subchannel is given by,

$$\tilde{\Gamma}_{k,E} = 2^{\frac{1}{N_k}\sum_{n=1}^{N_k}\log_2\left(1+\tilde{\Gamma}_k(n)\right)} - 1 \tag{3.15}$$

where N_k is the total number of data subcarriers in kth subchannel and $n \in \{1,2,3,.....N_k\}$. In our power allocation strategy, each subcarrier within a subchannel will experience the same SNR. If their SNR are not the same, then diffrent subcarriers will show different symbol error rate (SER). As a result complication arises in keeping FBER under a certain level. Let Φ_k be the allocated power to the kth subchannel, excluding the power of the pilot subcarriers. According to our power allocation strategy, Φ_k is distributed among the member subcarriers in such a way that

$$\frac{s_k(1)\left|\overline{\tilde{H}_k(1)}\right|^2}{\sigma^2} = \frac{s_k(2)\left|\overline{\tilde{H}_k(2)}\right|^2}{\sigma^2} = \frac{s_k(3)\left|\overline{\tilde{H}_k(3)}\right|^2}{\sigma^2} = \ldots\ldots\ldots\ldots = \tilde{\Gamma}_k(n) \tag{3.16}$$

$$\sum_{n=1}^{N_k} s_k(n) = \Phi_k \tag{3.17}$$

The equations (3.15) and (3.16) give us the following,

$$\tilde{\Gamma}_k(n) = \frac{\Phi_k}{\sum_{n=1}^{N_k} \frac{\sigma^2}{\left|\overline{\tilde{H}_k(n)}\right|^2}} \tag{3.18}$$

$$\tilde{\Gamma}_{k,E} = 2^{\frac{1}{N_k} N_k \log_2\left(1+\tilde{\Gamma}_k(n)\right)} - 1 = \tilde{\Gamma}_k(n), \qquad \forall n \tag{3.19}$$

Therefore, the effective SNR of the subchannel is equal to the estimated SNR of individual data subcarrier. One important fact is that there are some subcarriers, who are used as both pilot and data. We call them dual subcarriers. Dual subcarriers change their act based on symbol parity as described in the introductory paragraph of the current section. We consider each pair of alternative dual subcarriers as a single data subcarrier, whose channel response is just the simple average of the dual subcarriers' channel response. For example, the 1st and the 5th subcarriers of each cluster form a pair of alternative dual subcarriers. For odd symbols, the 1st subcarrier acts as pilot and the 5th subcarrier acts as data subcarrier. On the other hand for even symbols, the 5th subcarrier acts as pilot and the 1st subcarrier acts as data subcarrier. Similarly, the 9th and the 13th subcarriers of each cluster forms a pair of alternative dual subcarriers.

3.1.4 Relationship with the Estimated Post-Detection SNR

The relationship between the estimated SNR ($\tilde{\Gamma}_k(n)$) and the estimated post-detection SNR plays very important role in our LA algorithm. We need to construct an SNR threshold table based on this relationship. We have a 2×2 MIMO configuration.

In case of the STBC mode with MRC reception, the post-detection SNR of the n^{th} subcarrier of the k^{th} subchannel can be expressed as,

$$\tilde{\Gamma}_{k,STBC}(n) = \frac{s_k(n)\left\|\tilde{\mathbf{H}}(n)\right\|_F^2}{2\sigma^2}$$

$$= \frac{4\left|\overline{\tilde{H}_k(n)}\right|^2 s_k(n)}{2\sigma^2} \qquad \text{(Using equation (3.13))}$$

$$= 2\tilde{\Gamma}_k(n) \qquad (3.20)$$

In the case of SM with ZF detection, the post-detection SNR of the n^{th} subcarrier of the k^{th} subchannel can be expressed as (please see Appendix I),

$$\tilde{\Gamma}_{k,SM}(n) = \frac{s_k(n)\left|\Delta(n)\right|^2}{\sigma^2\left\|\tilde{\mathbf{H}}(n)\right\|_{\mathbf{F}}^2}$$

$$= \frac{s_k(n)\left|\overline{\tilde{H}_k(n)}\right|^2}{\sigma^2\left|\overline{\tilde{H}_k(n)}\right|^2}\frac{\left|\Delta(n)\right|^2}{\left\|\tilde{\mathbf{H}}(n)\right\|_{\mathbf{F}}^2}$$

$$= \frac{4\left|\Delta(n)\right|^2}{\left\|\tilde{\mathbf{H}}(n)\right\|_{\mathbf{F}}^4}\tilde{\Gamma}_k(n) \qquad (3.21)$$

$$= 4\tilde{\psi}_k(n)\tilde{\Gamma}_k(n) \qquad (3.22)$$

Here we define a multiplying factor, $\psi(n) = \frac{|\Delta(n)|^2}{\|\mathbf{H}(n)\|_{\mathbf{F}}^4}$ (3.23)

for any subcarrier n and $\tilde{\psi}_k(n)$ as an estimated version of $\psi_k(n)$ for $n \in \{1, 2, 3, ...N_k\}$.

One significant fact is that equation (3.22) contains the determinant ($\Delta(n)$) of the estimated channel matrix. Since the determinant is a measure of channel correlation; the channels should be sufficiently uncorrelated for the SM mode. Higher value of $\psi(n)$ indicates lower correlation and vice versa. We discuss more on this multiplying factor in subsection 3.2.2.

3.2 Selection of SNR Threshold

We need to construct an SNR threshold table. The table will indicate the minimum SNRs required to the corresponding burst profiles. These thresholds are selected based on modulation order, coding scheme and MIMO transmission mode. Higher order modulation demands higher SNR threshold and vice versa. In table 2.1, we saw that 16-QAM ¾ and 64-QAM ½ have the same spectral efficiency. As 64-QAM ½ uses higher modulation order, its SNR threshold is higher than that of 16-QAM ¾. For this reason, we exclude 64-QAM ½ with STBC and 64-QAM ½ SM from the list of the possible burst profiles. It is evident from the literature that the STBC mode performs better in the lower SNR region and the SM mode performs better in the higher region SNR. The main advantage of SM mode is that it increases spectral efficiency. We deploy the SM mode for spectral efficiency 4 or higher, i.e., we do not consider QPSK ½ and QPSK ¾ for the SM mode.

Based on the discussion above, we define two sets of burst profiles, one for STBC and another for SM.

$U_{STBC} := \{\text{QPSK1/2, QPSK3/4, 16-QAM1/2, 16-QAM3/4, 64-QAM2/3, 64-QAM3/4}\}$

$U_{SM} := \{\text{16-QAM1/2,16-QAM3/4, 64-QAM2/3, 64-QAM3/4}\}$

We set the SNR thresholds based on FBER upper bound. The upper bound of FBER is expressed by equation (2.8) of chapter 2. The upper bound based threshold selection provides better safety margin and lower computational cost. In threshold selection, we do not include SNR gain from convolution code (CC) scheme. Inclusion of this SNR gain corresponds to a higher BER tolerance, which sets a lower threshold for the same level of FBER. As a result the system vulnerability is increased and the safety margin is reduced. However, we include the impact of reduction in actual data block size. We select the SNR threshold values for FBER $\leq 10^{-3}$. Two tables are prepared to specify the minimum SNRs per symbol required to maintain FBER $\leq 10^{-3}$.

3.2.1 Threshold Table for STBC

We set the threshold values for STBC mode based on the FBER versus SNR per symbol plots shown in Fig. 3.2.

The threshold values for different burst profiles are summarized in Table 3.1.

Table 3.1: SNR threshold table for STBC mode, FBER $\leq 10^{-3}$.

Modulation	**CC Coding rate**	**MIMO mode**	**Bit /Symbol**	**Spectral Efficiency bps/Hz**	**SNR Threshold dB**
QPSK	½	STBC	2	1	12.5
QPSK	¾	STBC	2	1.5	14
16 QAM	½	STBC	4	2	23
16 QAM	¾	STBC	4	3	25
64 QAM	2/3	STBC	6	4	31
64 QAM	¾	STBC	6	4.5	32.5

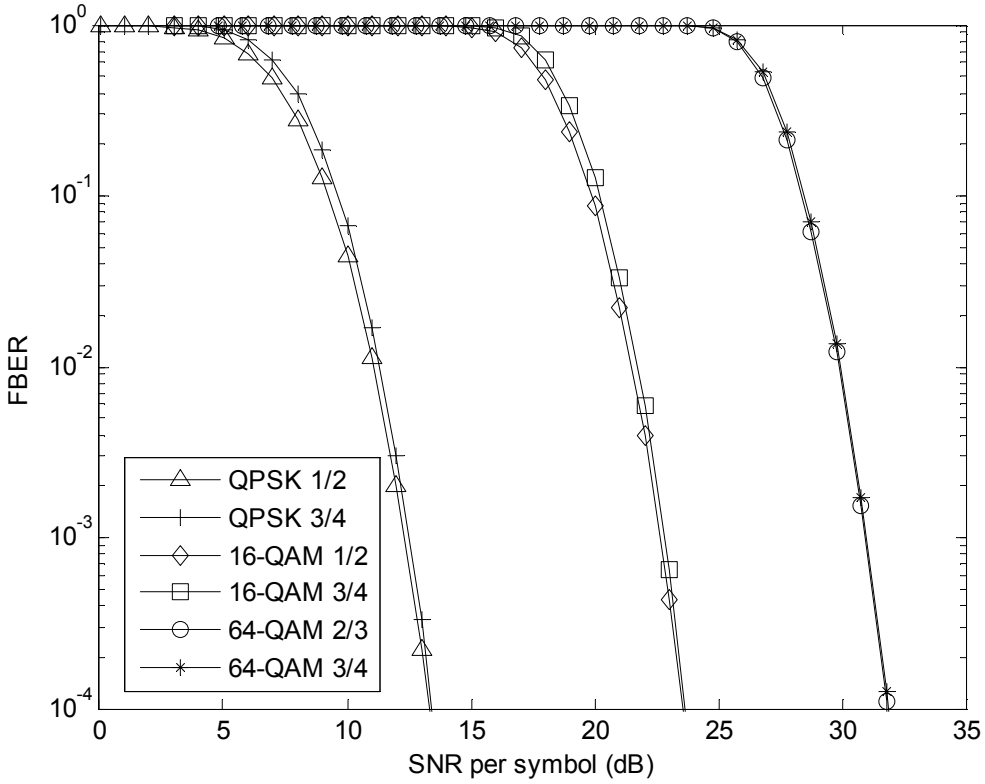

Fig. 3.2 FBER versus SNR plots for the STBC mode.

3.2.2 Threshold Table for SM

The threshold selection procedure for the SM mode is a little bit more complicated compared to that of the STBC mode. It requires some information on spatial correlation of the MIMO channels. From equation (3.22), we see that post-detection SNR of the SM mode not only depends on $\Gamma(n)$ but also on the multiplying factor $\psi(n)$. Basically, $\psi(n)$ is a measure of spatial correlation. In the literature, the Demmel condition number is widely accepted as the measure of spatial correlation [13], [28]. The Demmel condition number of a channel matrix $\mathbf{H}$ is given by,

$$C_D = \left\|\mathbf{H}\right\|_{\mathbf{F}} \left\|\mathbf{H}^{-1}\right\|_2 \tag{3.24}$$

where $\left\|\mathbf{H}^{-1}\right\|_2$ is the Euclidean norm of the inverse of the channel matrix $\mathbf{H}$. Actually, C_D tells us how invertible a channel matrix is. It decreases when the channel matrix is highly invertible. Higher value of C_D indicates higher correlation and vice versa. Therefore, ψ ($= |\Delta|^2 / \|\mathbf{H}\|_{\mathbf{F}}^{\ 4}$) has an inverse relationship with C_D. We generate 10,000 complex 2×2 random matrices using MATLAB [29], whose elements are independently Gaussian distributed random variables with zero mean and unit variance. We summarize our observations in Fig. 3.3. The multiplying factors ψ are on the x-axis, corresponding C_D are on the y-axis and the cumulative distribution function (CDF) of ψ is on the z-axis. The inverse relationship between ψ and C_D is clear to us.

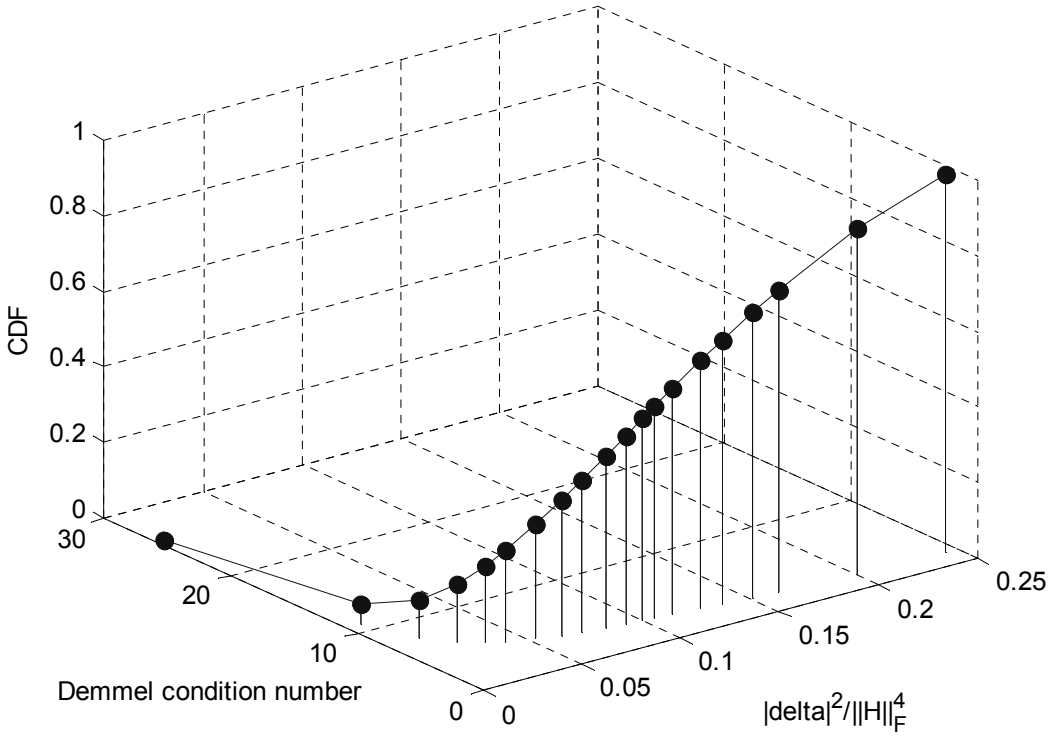

Fig. 3.3 CDF of ψ and corresponding C_D.

We have extracted some numerical values from the plot of Fig. 3.3, as shown in Table 3.2.

Table 3.2: Multiplying factor (ψ) summary.

Event Description (lower bound)	**Probability (approximate)**	**Maximum C_D (approximate)**
$\psi \geq 0.053$	0.70	4.2
$\psi \geq 0.1$	0.47	3
$\psi \geq 0.15$	0.25	2.3
$\psi \geq 0.2$	0.09	1.9

We need to select a lower bound for ψ and then based on that lower bound, the SNR threshold values can be selected. There is a tradeoff relationship between ψ and the threshold; higher value of ψ will reduce SNR threshold and lower value of ψ will increase SNR threshold. Also the lower bound should expose good chance of occurrence. Considering all these facts, we have decided to use $\psi \geq 0.1$, which exposes a good chance (47%) in our study. By choosing this lower bound we can keep C_D below 3.

We consider two conditions for SM mode to select the SNR threshold: FBER $\leq 10^{-3}$ and $\psi \geq 0.1$. We set the threshold values for the SM mode based on the FBER versus SNR per symbol plots shown in Fig. 3.4.

The threshold values for different burst profiles are summarized in Table 3.3.

Table 3.3: SNR threshold table for SM mode, FBER $\leq 10^{-3}$ and $\psi \geq 0.1$.

Modulation	**CC Coding rate**	**MIMO mode**	**Bit /Symbol**	**Spectral Efficiency bps/Hz**	**SNR Threshold dB** ($\psi \geq 0.1$)
16 QAM	½	SM	4	4	30
16 QAM	¾	SM	4	6	31
64 QAM	2/3	SM	6	8	38
64 QAM	¾	SM	6	9	39

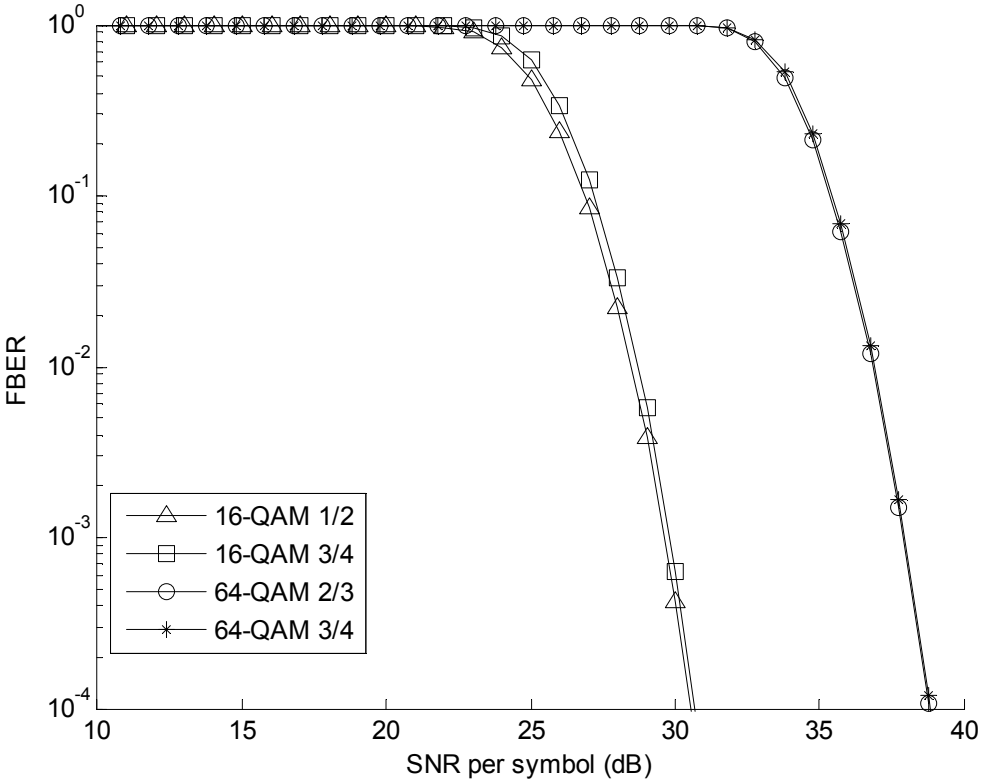

Fig. 3.4 FBER versus SNR plots for the SM mode.

3.3 LA Algorithm for Mobile Hotspot

Though we have not found any exact match of our problem and system combination in the literature, we discuss the ramifications of some previously proposed LA techniques for mobile WiMAX. These discussions will help us to differentiate our proposed LA algorithm from the others. We select three techniques because they deal with similar problems as ours. A static threshold table based LA is proposed in [30], which is the simplest technique. The table is prepared based on pedestrian channel model and target FBER. The table indicates the threshold SNRs for the different burst profiles. This LA technique requires only the SNR information to select an appropriate burst profile. The important issues like higher mobility, MIMO channel correlations, error tracking, etc, are ignored. The Moore's finite state based LA technique is proposed in [31]. Each burst profile represents a state. Basically they propose two separate LA techniques: channel

state technique and error technique. In the channel state technique, an attenuation factor is used to select burst profile. This approach is theoretical rather than practical. In the error technique, the number of successive erroneous frames is used to select burst profile. It selects lower order modulation if a certain number of failure deliveries occurs. And, selects higher order modulation if a certain number of successful deliveries occurs. The MIMO features and channel coding are ignored in both techniques. Moreover, the system becomes complicated as the number of states increases. A dynamic threshold LA (DTLA) algorithm is proposed in [32]. It dynamically sets and updates the SNR thresholds for different burst profiles. It selects an appropriate burst profile based on SNR threshold and Demmel condition number. There is no error tracking mechanism such as ARQ being considered in DTLA. Their algorithm is not high mobility specific. The DTLA algorithm consists of many feedback loops, which are computationally expensive. Though it adopted an "SNR adjustment step" from the IEEE 802.16e standard [1], it does not reveal how the adjustment factor is set. It also ignores the subchannelization and the power allocation issues.

Our deemed LA algorithm uses a static threshold table of SNR per symbol. But we dynamically adjust the SNR before looking at the table. This adjustment is done based on mobility state. Our algorithm also considers MIMO channel correlation. We consider an adaptive ARQ mechanism for error tracking.

3.3.1 Throughput Maximization

In section 2.6 of chapter 2, we addressed a throughput maximization problem. In the next subsection, we propose a solution for that problem. The solution is nothing but our LA algorithm. Without using the traditional nonlinear optimization techniques, we can solve it heuristically. The main idea is that "if we select the burst profile with the highest spectral efficiency at a given condition, then the throughput will be maximized." It is an easy task to do for the ideal cases. In an ideal case, the channel estimation is perfect; MIMO channels are totally uncorrelated and there is no erroneous reception, etc. Unfortunately, we have to consider a realistic case. In order to adapt with the realistic

scenario, we set a constraint named “priority function” in the problem formulation. The NACK message or erroneous reception occurs when SNR is over estimated. The priority function affects the burst profile selection and works as a protection against successive erroneous reception. The solution automatically contains an adaptive ARQ mechanism due to the priority function.

3.3.2 The proposed LA Algorithm

Before describing our LA algorithm steps, we reiterate some conditions: subchannel allocation and inter subchannel power allocation are done by the resource allocation algorithm. We do not have anything to do with those matters. Our algorithm starts from when a subchannel is allocated to a mobile hotspot and the power for that subchannel is also allocated. Intra subchannel power allocation for our algorithm has been described in subsection 3.1.3. Here we describe how an appropriate burst profile is selected for a subchannel. Our goal is to perform frame by frame link adaptation for downlink.

The flow diagram of the proposed LA algorithm is shown in Fig. 3.5.

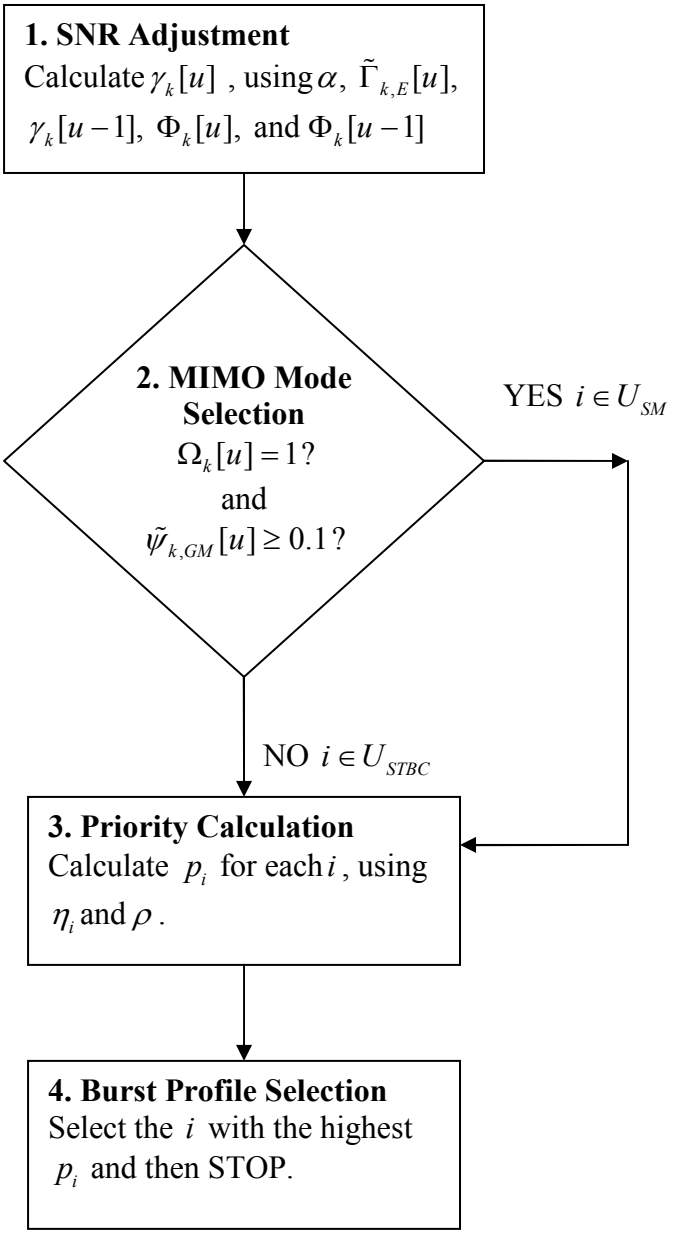

Fig. 3.5 Flow diagram of the proposed LA algorithm.

The following are the descriptions of the different symbols used in the flow diagram:

- $\gamma_k[u]$ is the adjusted SNR of the k^{th} subchannel for the u^{th} downlink subframe.
- $\gamma_k[u-1]$ is the adjusted SNR of the k^{th} subchannel for the $(u-1)^{th}$ downlink subframe.
- α is the adjustment factor

- $\tilde{\Gamma}_{k,E}[u]$ is the estimated effective SNR of the k^{th} subchannel for the u^{th} downlink subframe.
- $\Phi_k[u]$ is the allocated power to the k^{th} subchannel for the u^{th} downlink subframe.
- $\Phi_k[u-1]$ is the allocated power to the k^{th} subchannel for the $(u-1)^{th}$ downlink subframe.
- $\Omega_k[u]$ is the MIMO threshold function of the k^{th} subchannel for the u^{th} downlink subframe.
- ρ is the ARQ message indicator.
- $\tilde{\psi}_{k,GM}[u]$ is the geometric mean of the estimated multiplying factors of the k^{th} subchannel for the u^{th} downlink subframe.
- U_{SM} is the set of the candidate burst profiles for the SM mode
- U_{STBC} is the set of the candidate profiles for the STBC mode.
- i is the burst profile index
- p_i is the priority function of the burst profile i
- η_i is the spectral efficiency of the burst profile i

We see that the proposed algorithm is straightforward and unidirectional. There is no feedback loop in the flow diagram. This indicates the simplicity of the proposed algorithm. The proposed LA algorithm works as follows:

Step 1: SNR adjustment

An OFDMA frame starts with a downlink subframe and ends with an uplink subframe. A time gap interval takes place between them. The downlink burst profiles are selected based on the feedback information from the previous uplink. We need to adjust the estimated SNR due to high mobility. We define an adjusted SNR of the k^{th} subchannel for the u^{th} downlink subframe as

$$\gamma_k[u] = (1-\alpha)\tilde{\Gamma}_{k,E}[u] + \alpha \frac{\gamma_k[u-1]\Phi_k[u]}{\Phi_k[u-1]}, \qquad \alpha \in [0,1] \tag{3.25}$$

where adjustment factor $\alpha = \frac{v_{current}}{v_{\max}}$ (please see Appendix II)

$v_{current}$ is the current velocity of the mobile hotspot.

$v_{\max}$ is the maximum velocity of the mobile hotspot.

We know that SNR depends on the allocated power. The allocated power may not be the same for every downlink subframe. Therefore, we need to extract the channel factor from $\gamma_k[u-1]$ and then calculate an equivalent SNR for $\Phi_k[u]$. That is why $\gamma_k[u-1]$ is multiplied by the ratio $\frac{\Phi_k[u]}{\Phi_k[u-1]}$ in the second term of equation (3.25).

Step 2: MIMO mode selection

We know that the STBC mode performs better in the lower SNR region and the SM mode performs better in the higher SNR region. But SNR information is not enough for the SM mode, it requires an additional information on ψ. Therefore, we consider both of them in our mode selection procedure. The geometric mean of the estimated multiplying factors ($\tilde{\psi}$) of the k^{th} subchannel for the u^{th} downlink subframe is given by

$$\tilde{\psi}_{k,GM}[u] = \left[\prod_{n=1}^{N_k} \tilde{\psi}_k(n)\right]^{\frac{1}{N_k}} \tag{3.26}$$

We need to define a function in order to specify SNR information of a particular subchannel for a particular downlink subframe. We call it the MIMO threshold function. The MIMO threshold function of the k^{th} subchannel for the u^{th} downlink subframe is defined as

$$\Omega_k[u] = I_{\{\rho=0\}} I_{\{\gamma_k[u] \geq 30 \text{ dB}\}} + I_{\{\rho=1\}} I_{\{\gamma_k[u] \geq 31 \text{ dB}\}} \quad (3.27)$$

$I_{\{\}}$ is the indicator function which takes either 1 or 0 depending on satisfaction of condition.

ρ takes 0 if the corresponding ARQ block in the previous downlink subframe was successfully received and 1 for erroneous reception.

The MIMO threshold function prevents the formation of feedback loop i.e., we do not need to change the MIMO mode once we select it for a particular downlink subframe. $\Omega_k[u]$ specifies two thresholds for the SM mode depending on the ARQ message indicator: 30 dB for $\rho = 0$ and 31 dB for $\rho = 1$.

In a simple manner we can say, if $\Omega_k[u] = 1$ and $\tilde{\psi}_{k,GM}[u] \geq 0.1$, then select the SM mode. Otherwise select the STBC mode. In the SM mode, the possible burst profile i is chosen as $i \in U_{SM}$. In the STBC mode, the possible burst profile i is chosen as $i \in U_{STBC}$.

Step 3: Priority Calculation

The priorities of the burst profile can be calculated by using a modified version of equations (2.12a) and (2.12b). Here we use the corresponding SNR threshold instead of FBER. Higher value of the priority function indicates higher spectral efficiency and vice versa.

$$p_i(\eta_i, \rho) = \eta_i I_{\{\gamma_k[u]) \geq \theta_i\}} [I_{\{\text{i}=\arg\max_{\text{j}} \eta_j I_{\{\gamma_k[u] \geq \theta_j\}}\}} I_{\{\rho=0\}} + I_{\{\text{i}\neq\arg\max_{\text{j}} \eta_j I_{\{\gamma_k[u] \geq \theta_j\}}\}} I_{\{\rho \geq 0\}}] \quad (3.28a)$$

$$\text{for } \sum_{i}^{U} I_{\{\gamma_k[u]) \geq \theta_i\}} \geq 2$$

$$= \eta_i I_{\{\gamma_k[u]) \geq \theta_i\}} \qquad \text{for } \sum_{i}^{U} I_{\{\gamma_k[u]) \geq \theta_i\}} = 1 \quad (3.28b)$$

θ_i is the SNR threshold of the burst profile i

η_i is the spectral efficiency of the burst profile i

$I_{\{\}}$ is the indicator function it takes either 1 or 0 depending on satisfaction of condition.

ρ takes 0 if the corresponding ARQ block in the previous downlink subframe was successfully received and 1 for erroneous reception.

i, j are the indices for the burst profiles

Step 4: Burst profile selection

The final step is to select the burst profile with the highest priority.

$$i^* = \arg \max_i \; p_i(\eta_i, \rho) \tag{3.29}$$

As the priority function assigns higher priorities to the higher spectral efficiency burst profiles, the burst profile i^* will maximize throughput. We repeat the same routine for each subchannel to find the optimum burst profile.

Chapter 4

Numerical Results

In this chapter we present some numerical results on the proposed LA algorithm. These results are obtained from downlink link level simulations using partial Monte Carlo method in MATLAB [33], [34]. We consider some simple scenarios, which are appropriate for evaluating performance of the proposed LA algorithm. We consider a single cell single user (only one mobile hotspot) case through out this thesis. The downlink exists between a WiMAX BS and the AP of a mobile hotspot is simulated. Basically, there are two performance metrics: FBER and normalized throughput are evaluated. We define an ARQ block which consists of one subchannel and two time slot. We choose two nonadjacent physical clusters to construct the subchannel. The simulation parameters are summarized in Table 4.1. The miscellaneous losses include the AP noise figure and any other possible losses.

Though the ARQ block is a small part of the whole downlink subframe, we use the term frame to mean the ARQ block for convenience. We have already described the SNR estimation and the intra subchannel power allocation procedure in chapter 3. There are four major categories of investigations are presented: impact of moving direction, impact of velocity, impact of velocity based SNR adjustment, and impact of adaptive ARQ. Before discussing the numerical results, we would like to review some important facts about the simulated channel. The numerical results are highly dependent on the channel specifications.

Table 4.1: Simulation parameters

Parameter	Description/Value
Cell radius	1 km
Allocated power to the subchannel	0.5 Watt, 1.0 Watt
BS Antenna gain	16 dBi
BS Antenna height	40 m
Frequency band	2.3 GHz
FFT size	1024
System bandwidth	10 MHz
Symbol duration	115.2 μs
Guard ratio	1/8
Thermal noise density	-174 dBm/Hz (at 25^0 C)
Mobile hotspot velocity	60 km/hr, 90 km/hr, 120 km/hr
Subchannelization strategy	PUSC
Duplex mode	TDD
Channel model	ITU-R Vehicular B
AP antenna height	2.8 m
Shadowing loss	10 dB
Path loss model	COST 231 Hata model for suburban environment (min. separation required 35 m)
Miscellaneous losses	10 dB
AP Antenna gain	8 dB
Fading type	Flat Rayleigh fading
Frame duration	5 ms
DL to UL ratio	3:1
MIMO Antenna configuration	2×2
MIMO mode	STBC, SM (switchable)
Burst size (one ARQ block)	1 subchannel × 4 symbols
Maximum number of retransmissions	3
$v_{\max}$ settings	360 km/hr

4.1 Channel Description

We consider a suburban environment. Usually, vehicle velocity in the urban or metropolitan areas is restricted under certain range. The suburban environment is feasible for high velocity vehicle. We select the BS height 40 meter; the AP antenna height is 2.8 meter, and the carrier frequency 2.3 GHz. In this case, the COST 231 Hata path loss model is reduced to:

$$PL = 37 + 34.4 \log_{10}(d) \text{ dB} \tag{4.1}$$

where d is the distance between the WiMAX BS and the mobile hotspot AP in meters. Equation (4.1) is valid for $d \geq 35$ meter [14].

The WiMAX forum recommends to consider 10 dB shadowing loss for simulation of the mobile WiMAX. We just follow this recommendation for shadowing loss [15].

The multipath propagation is simulated using ITU-R vehicular channel model B [35]. The channel specification is shown in the Table 4.2. This model is valid for the velocity between 60 km/hr to 120 km/hr.

Table 4.2: ITU-R Vehicular channel model B.

Path No.	Relative Delay (ns)	Average Power (dB)	Doppler spectrum
1	0	-2.5	Classic
2	300	0	Classic
3	8900	-12.8	Classic
4	12900	-10.0	Classic
5	17100	-25.2	Classic
6	20000	-16.0	Classic

Channel response of each path is modeled as independent complex Gaussian random variable with zero mean and unit variance. As a result, the envelopes of the channel responses can be considered as independently Rayleigh distributed random variables with unit variance. The time correlation between two consecutive samples of channel response of path l is given by [36],

$$\beta_l = \begin{cases} J_0(2\pi f_{D,l}\Delta t) & \text{for } \Delta t \le T_c \\ 0 & \text{for } \Delta t > T_c \end{cases} \tag{4.2}$$

where $J_0(\,)$ is the zero order Bessel function of the first kind., $f_{D,l}$ is the maximum Doppler frequency of path l, Δt is the elapsed time between two samples, and T_c is the coherence time of the channel at a given frequency and velocity. The maximum Doppler frequency of path l , at carrier frequency f_c and velocity v, is given by

$$f_{D,l} = \frac{vf_c}{c} \tag{4.3}$$

where c is the velocity of light in free space. We consider the maximum Doppler shift of each path is the same. Then the coherence time is defined as [37],

$$T_c = \frac{0.423}{f_D} \tag{4.4}$$

where f_D is the maximum Doppler frequency at a given carrier frequency and velocity. Another important channel parameter is the classic Doppler power spectrum, which is also known as Clarke or Jakes spectrum [36], [38]. It is obtained from the Fourier transform of the time correlation of the channel response envelope. The Doppler power spectrum of a frequency difference Δf from the centre frequency is given by

$$S(\Delta f) = \begin{cases} \dfrac{1}{\pi f_D \sqrt{1 - \left(\dfrac{\Delta f}{f_D}\right)^2}} & \text{for } |\Delta f| \le f_D \\ 0 & \text{for } |\Delta f| > f_D \end{cases} \tag{4.5}$$

4.2 Impact of Moving Direction

We consider two cases of moving direction: (i) a mobile hotspot arriving to the cell centre (we call it the arriving mobile hotspot), and (ii) a mobile hotspot departing from the cell centre (we call it the departing mobile hotspot). In both cases the velocity is set to 90 km/hr, and the allocated power is set to 0.5 Watt (27 dBm). The initial distance for the arriving mobile hotspot is 900 meters from the BS. The initial distance for the departing mobile hotspot is 150 meters from the BS. Numerical results are obtained for 30 seconds duration (6000 frames).

Fig. 4.1(a) shows the instantaneous FBER plots for the arriving mobile hotspot. It reveals that, the proposed LA algorithm is able to keep the "instantaneous FBER" $\le 10^{-3}$ in most of the time (around 70%). We see some missing points between 15^{th} and 18^{th} second. This happens because MATLAB does not show the points below 10^{-15}. Actually, FBER is very low in this interval. It can be clear from the same interval of Fig. 4.1(b), since there is no severe degradation of throughput. Some frames exhibit very high FBERs between 24^{th} and 28^{th} second due to imperfect estimation of SNR and multiplying factor. Mostly, the SM mode is selected for these frames.

Fig. 4.1(b) shows the instantaneous normalized throughput plots for the arriving mobile hotspot. It reveals that, the throughput is dominated by the path loss. We see that throughput increases as the mobile hotspot getting closer to the BS. The path loss decreases with time for the arriving mobile hotspot. Throughput degrades severely in some frames between 24^{th} and 28^{th} second as the corresponding FBERs are very high in Fig. 4.1(a).

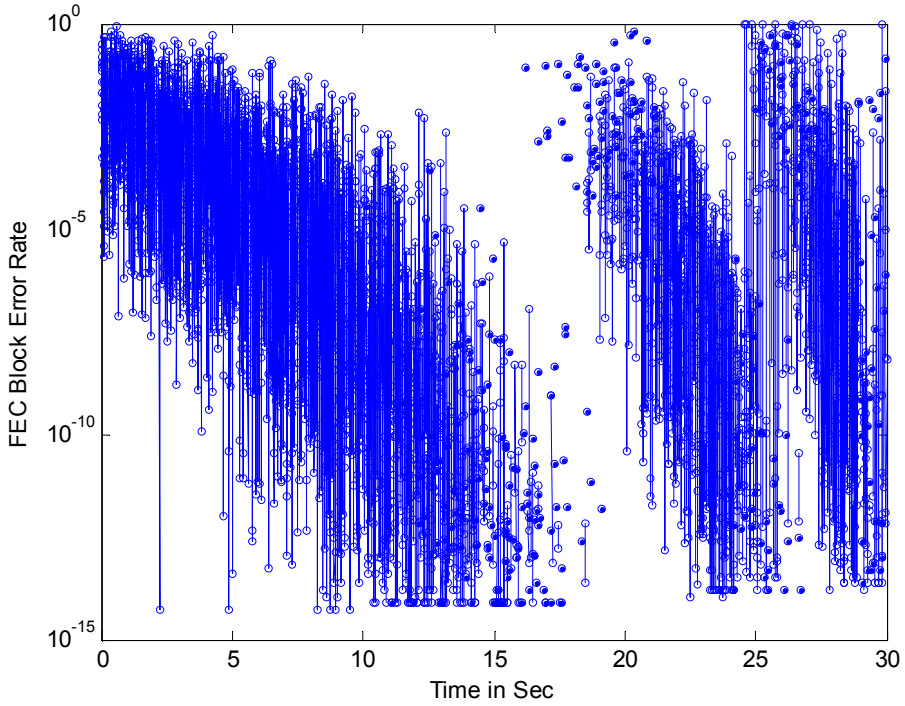

Fig. 4.1(a) Instantaneous FBER plots for the arriving mobile hotspot.

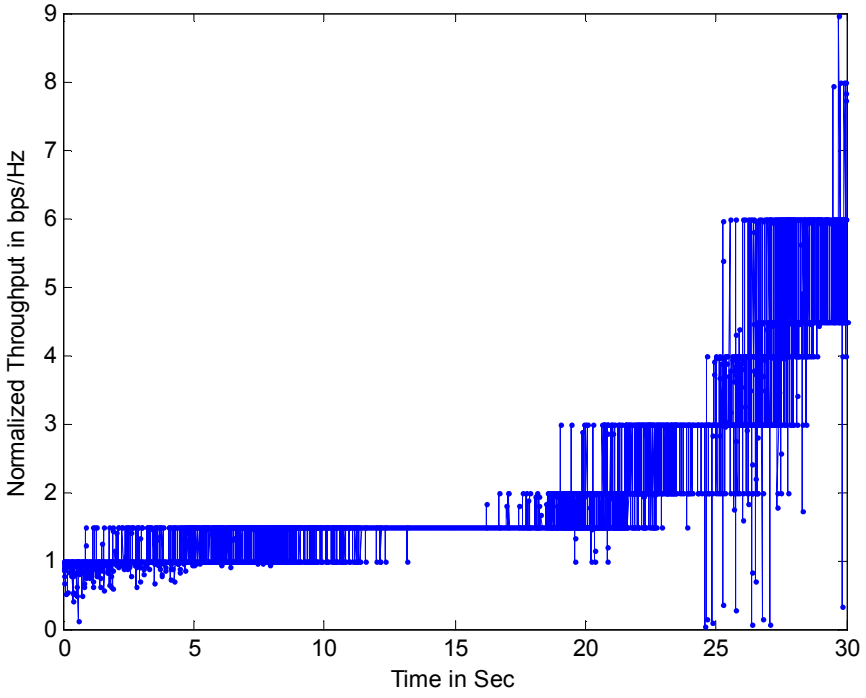

Fig. 4.1(b) Instantaneous normalized throughput plots for the arriving mobile hotspot.

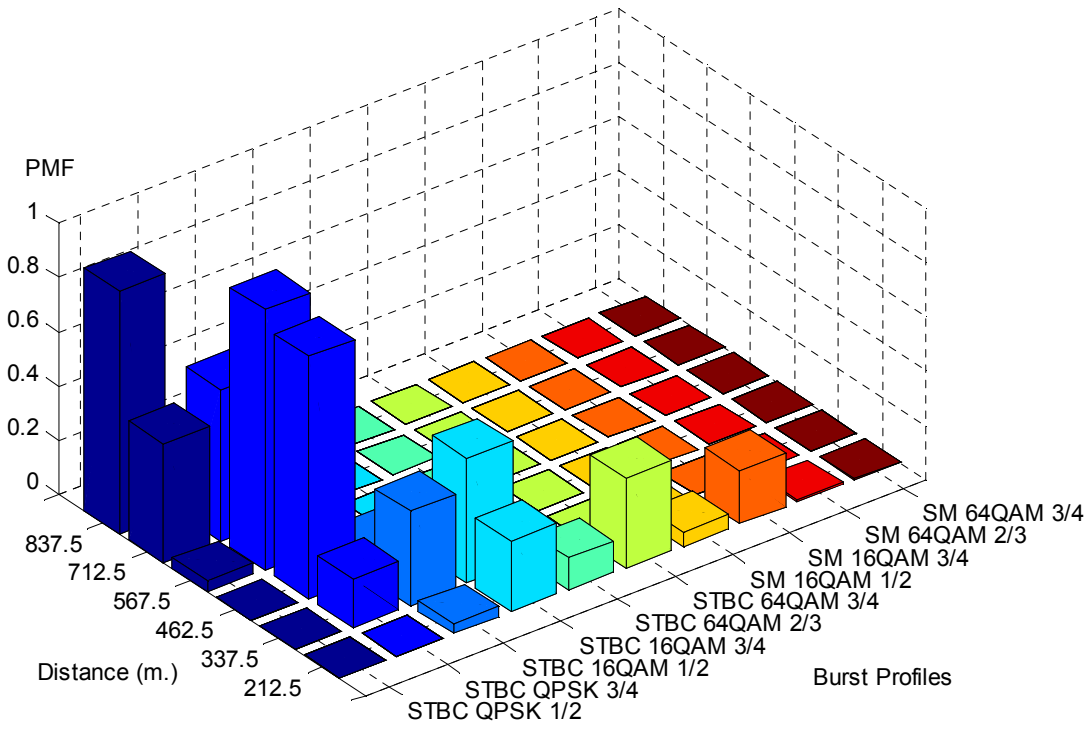

Fig. 4.1(c) PMF of the selected burst profiles for arriving direction at various distances.

The normalized throughput is 1.5 bps/Hz and below up to 16th second (about 500 m distance). Then it gradually increases to the higher values.

Fig. 4.1(c) shows the probability mass function (PMF) of the selected burst profiles at various distances for the arriving mobile hotspot. We see that, lower spectral efficiency burst profiles have very high PMF in the longer distances. Signals at longer distances experience lower SNR due to path loss. Therefore, lower spectral efficiency burst profiles are selected for longer distance. The higher spectral efficiency burst profiles expose higher PMF as the distance reduces. PMF of the SM mode burst profiles are negligible above 275 meters distance. The STBC mode is dominating all the way. The SM mode requires higher SNR and lower spatial correlation together. That is why the SM mode burst profiles have lower PMF.

Let us discuss on the departing mobile hotspot. Fig. 4.2(a) shows the instantaneous FBER plots for the departing mobile hotspot. It reveals that, the proposed LA algorithm is able

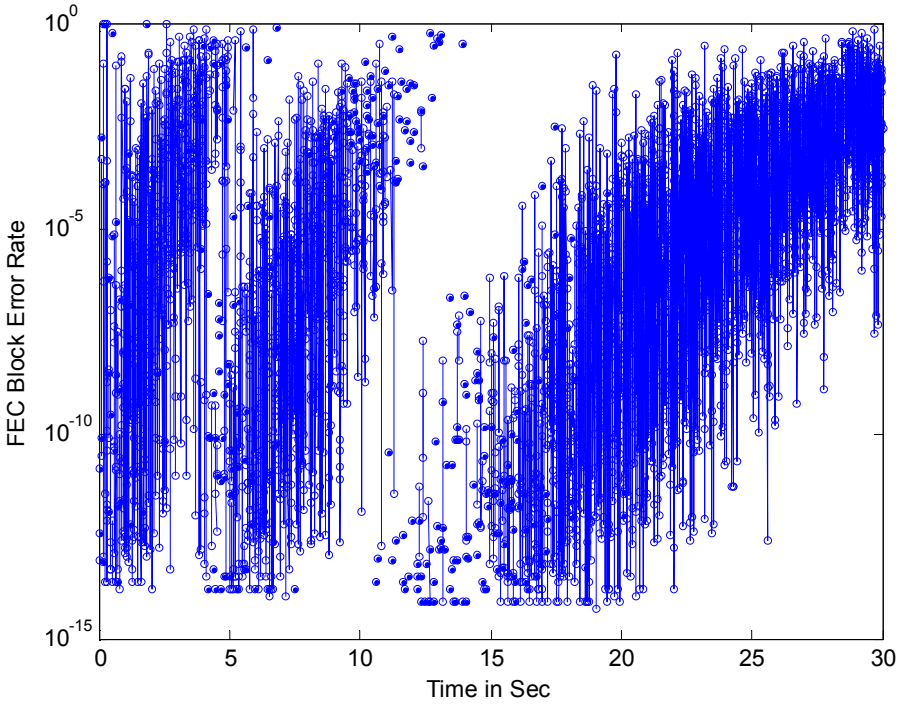

Fig. 4.2(a) Instantaneous FBER plots for the departing mobile hotspot.

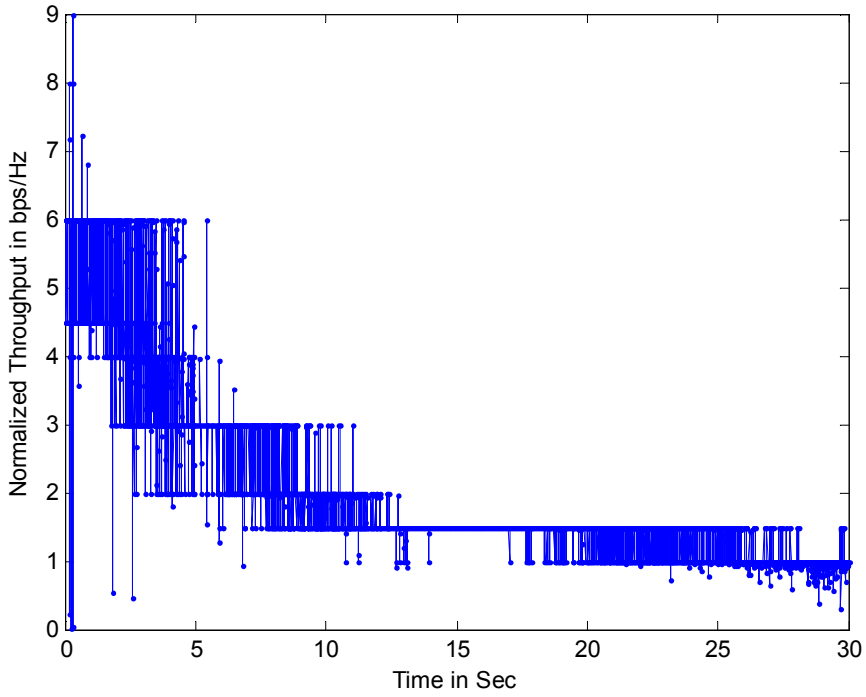

Fig. 4.2(b) Instantaneous normalized throughput plots for the departing mobile hotspot.

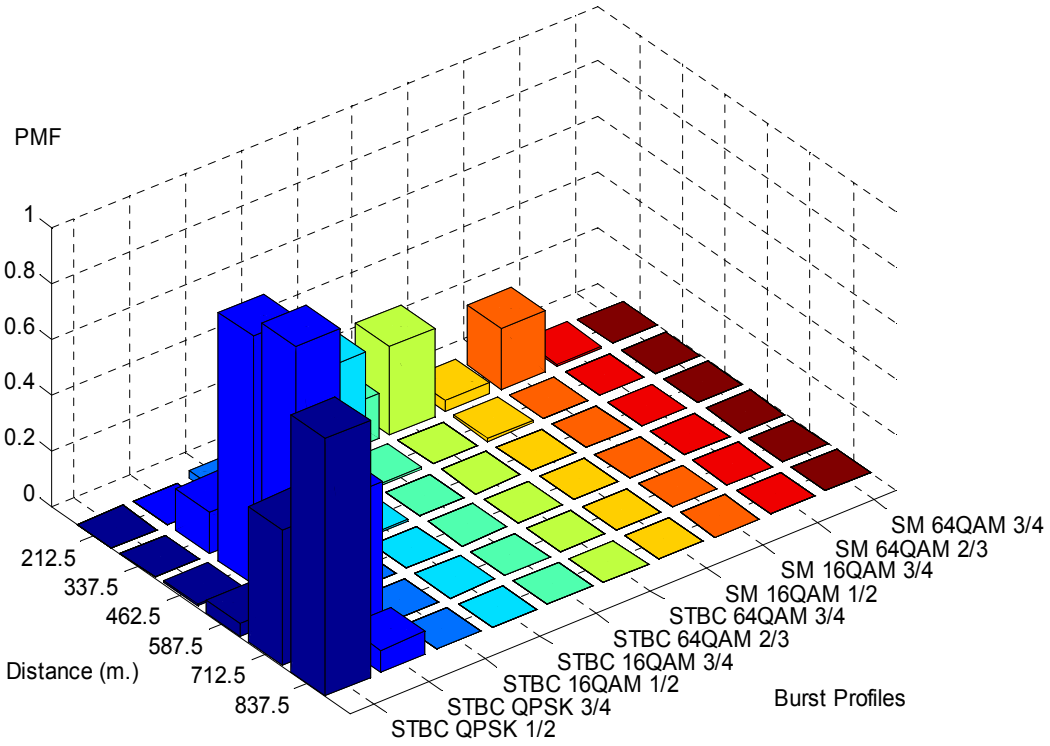

Fig. 4.2(c) PMF of the selected burst profiles for departing direction at various distances.

to keep the "instantaneous FBER" $\leq 10^{-3}$ in most of the time (around 80%). We see some missing points between 9^{th} and 16^{th} second due to the same reason as in Fig. 4.1(a).

Fig. 4.2(b) shows the instantaneous normalized throughput plots for the departing mobile hotspot. It reveals that, the throughput is dominated by the path loss. We see that throughput decreases as the mobile hotspot getting further from the BS. The path loss increases with time for the departing mobile hotspot. The normalized throughput degrades gradually up to 13^{th} second (about 475 meter distance). Then it becomes steady between 1.5 bps/Hz and below. Roughly, Fig. 4.2(b) shows a reverse scenario of Fig. 4.1(b) because of opposite moving directions.

Fig. 4.2(c) shows the probability mass function (PMF) of the selected burst profiles at various distances for the departing mobile hotspot. We see that, higher spectral efficiency (3.0 bps/Hz and above) burst profiles have very high PMF up to 275 meter distance. The SM mode burst profiles do not exhibit any significant PMF after 400 meter distance.

Signals at longer distances experience lower SNR due to path loss. Therefore, lower spectral efficiency burst profiles are selected for longer distances. The higher spectral efficiency burst profiles expose lower PMF as the distance increases.

4.3 Impact of Velocity

As the mobile hotspots are implemented on high velocity vehicles, it is important to investigate the impact of velocity. At first, we consider the departing mobile hotspot with three different velocities 60 km/hr, 90 km/hr and 120 km/hr. The allocated power is set to 1 Watt (30 dBm) for each. The initial distance is set to 200 meters from the BS. These mobile hotspots experience the same fading channel at the first symbol of each frame. Numerical results are obtained for 20 seconds duration (4000 frames). Since it is difficult to conclude from the instantaneous values, we take average of every 2 seconds interval.

Fig. 4.3(a) shows the average normalized throughput versus time interval plots for different departing velocities. Though the mobile hotspots experience the same fading channel at the first symbols, their velocities are different. As a result, time correlations of the frequency responses are different. The mobile hotspots experience different path losses because of different velocities. We see that throughput degrades with higher velocity. The mobile hotspots with higher velocities move faster from the BS compared to the lower velocities. Higher velocity mobile hotspot experience higher path losses at the same time. Impact of velocity is taken into account in our proposed LA algorithm by adjusting SNR. Thus burst profile selection is also affected by velocity. We will discuss on the impact of SNR adjustment in the next section.

Fig. 4.3(b) shows the average FBER versus time interval plots for different departing velocities. We see that the average FBER performance do not maintain the relative order of the average throughput performance. This happens because the different burst profiles exhibit different FBER. The proposed LA algorithm may select different burst profiles for different velocities even at the same SNR (without adjustment). The worst FBER

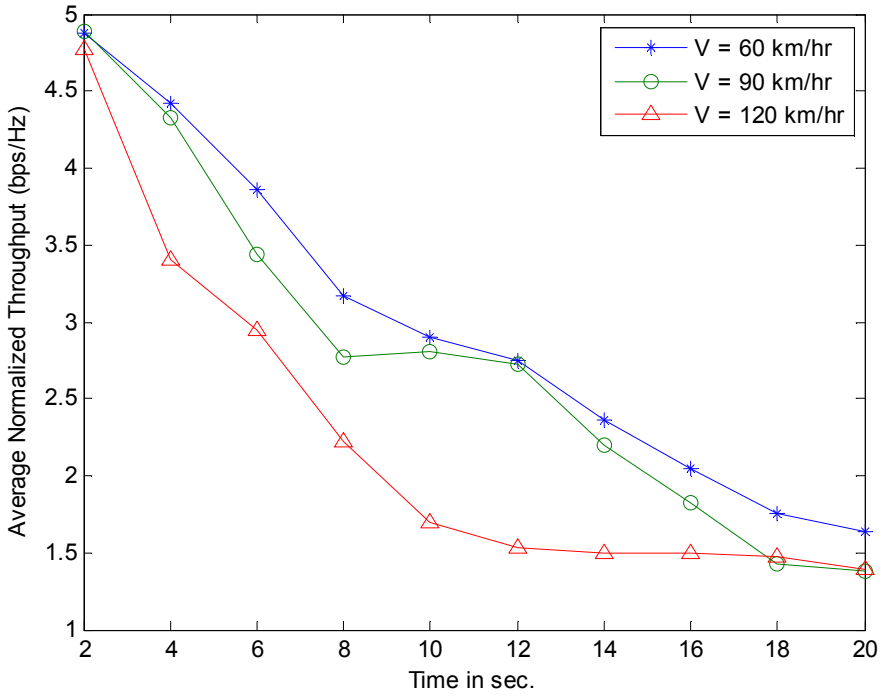

Fig. 4.3(a) Average normalized throughput comparison for different departing velocities.

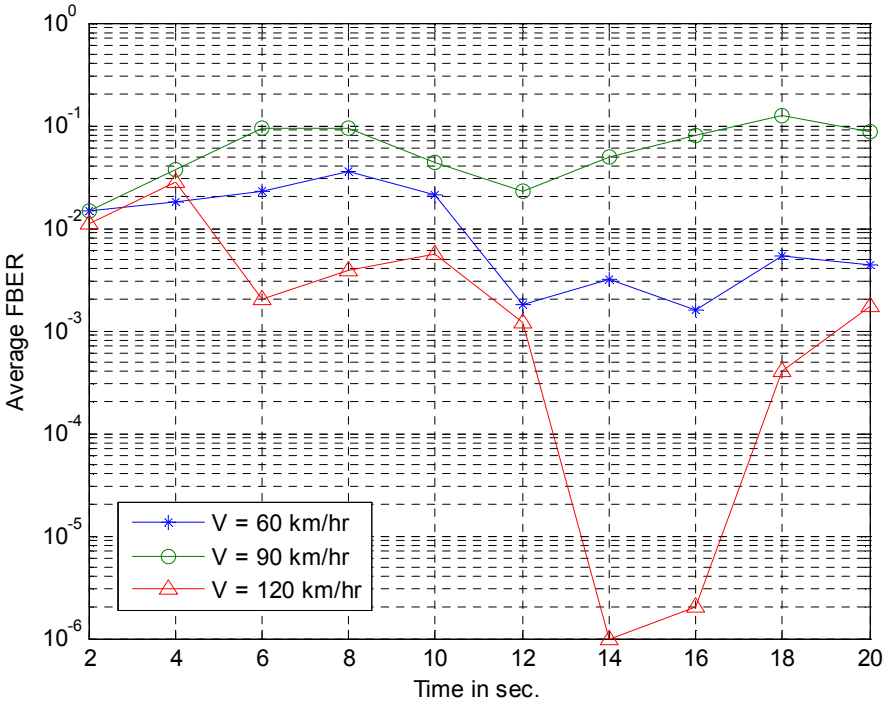

Fig. 4.3(b) Average FBER comparison for different departing velocities.

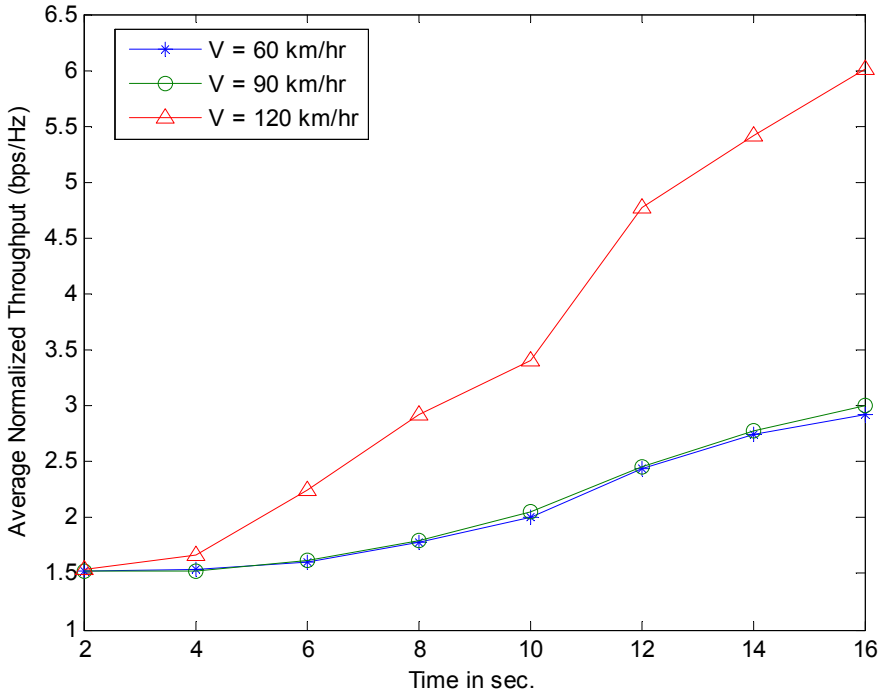

Fig. 4.4(a) Average normalized throughput comparison for different arriving velocities.

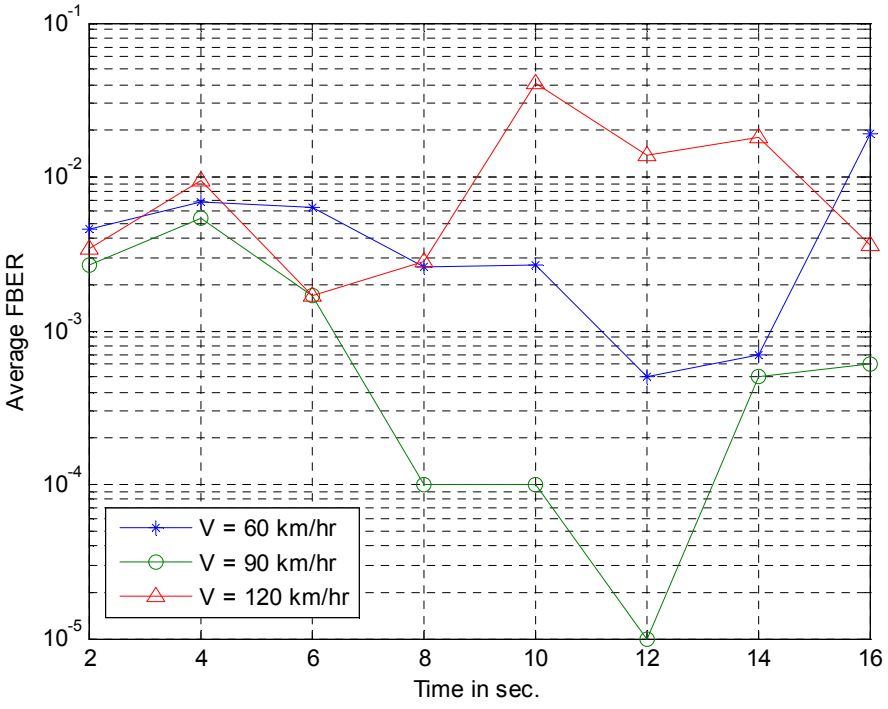

Fig. 4.4(b) Average FBER comparison for different arriving velocities.

performance is exhibited by the mobile hotspot with velocity 90 km/hr. The best FBER performance is exhibited by the mobile hotspot with velocity 120 km/hr. The mobile hotspot with velocity 60 km/hr exhibits a moderate FBER performance.

We also consider the arriving mobile hotspot with three different velocities 60 km/hr, 90 km/hr and 120 km/hr. The allocated power is set to 1 Watt (30 dBm) for each. The initial distance is set to 600 meters from the BS. These mobile hotspots experience the same fading channel at the first symbol of each frame. Numerical results are obtained for 16 seconds duration (3200 frames). Since it is difficult to conclude from the instantaneous values, we take average of every 2 seconds interval.

Fig. 4.4(a) shows the average normalized throughput versus time interval plots for different arriving velocities. We see the reverse scenario of Fig. 4.3(a), throughput improves with higher velocity. The mobile hotspots with higher velocities move faster to the BS compared to the lower velocities. Higher velocity mobile hotspot experience lower path losses at the same time. Throughput of mobile hotspot with velocity 120 km/hr increases very sharply, whereas with velocity 90 km/hr and 60 km/hr increase slowly. Their relative order is just the reverse of the departing mobile hotspot case.

Fig. 4.4(b) shows the average FBER versus time interval plots for different arriving velocities. We see that the average FBER performance do not maintain the relative order of the average throughput performance.

4.4 Impact of Velocity based SNR Adjustment

As the proposed LA algorithm adjusts SNR based on velocity of the mobile hotspots, it is necessary to investigate the impact of velocity based SNR adjustment. We separately consider three different cases of velocity 60 km/hr, 90 km/hr and 120 km/hr. These mobile hotspots are the departing mobile hotspots. The initial distance is set at 200 meters from the BS. The allocated power is set to 0.5 Watt (27 dBm) in each case. We

compare the performance of the SNR adjusted LA with that of the SNR non-adjusted LA (just omitting the first step of the proposed LA algorithm). We compare the average performance of every 2 seconds interval.

Firstly, we consider a mobile hotspot with velocity 60 km/hr. Numerical results are obtained for 25 seconds duration (5000 frames). Fig. 4.5(a) and Fig. 4.5(b) show the comparative throughput and FBER performance respectively. We see that velocity based SNR adjustment performs better than the non-adjusted SNR in both of the perspectives. The velocity based SNR adjustment improves throughput and reduces FBER. Overall average of the normalized throughput is 2.2154 bps/Hz for the velocity based SNR adjustment, whereas that for the non-adjusted SNR is 2.2045 bps/Hz. Overall average of the FBER is 0.0107 for the velocity based SNR adjustment, whereas that for the non-adjusted SNR is 0.0110.

Secondly, we consider a mobile hotspot with velocity 90 km/hr. Numerical results are obtained for 22 seconds duration (4400 frames). Fig. 4.6(a) and Fig. 4.6(b) show the comparative throughput and FBER performance respectively. We see that velocity based SNR adjustment performs better than the non-adjusted SNR in both of the perspectives. The velocity based SNR adjustment improves throughput and reduces FBER. Overall average of the normalized throughput is 1.9803 bps/Hz for the velocity based SNR adjustment, whereas that for the non-adjusted SNR is 1.9636 bps/Hz. Overall average of the FBER is 0.0081 for the velocity based SNR adjustment, whereas that for the non-adjusted SNR is 0.0095.

Thirdly, we consider a mobile hotspot with velocity 120 km/hr. Numerical results are obtained for 20 seconds duration (4000 frames). Fig. 4.7(a) and Fig. 4.7(b) show the comparative throughput and FBER performance, respectively. We see that velocity based SNR adjustment performs better than the non-adjusted SNR in both of the perspectives. The velocity based SNR adjustment improves throughput and reduces FBER. Overall average of the normalized throughput is 1.8225 bps/Hz for the velocity based SNR adjustment, whereas that for the non-adjusted SNR is 1.7929 bps/Hz. Overall average

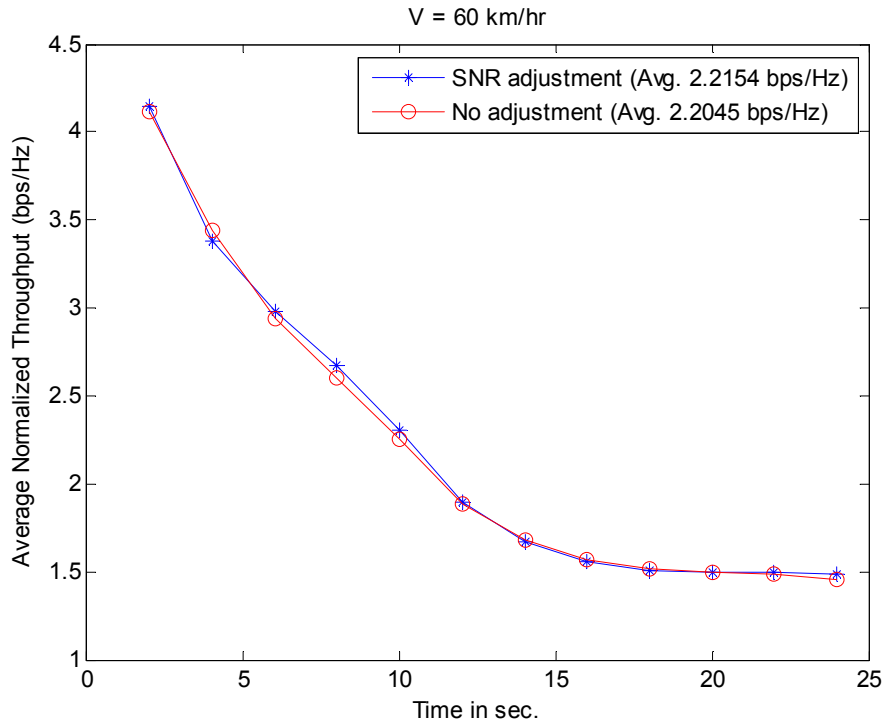

Fig. 4.5(a) Impact of SNR adjustment on the throughput with velocity 60 km/hr.

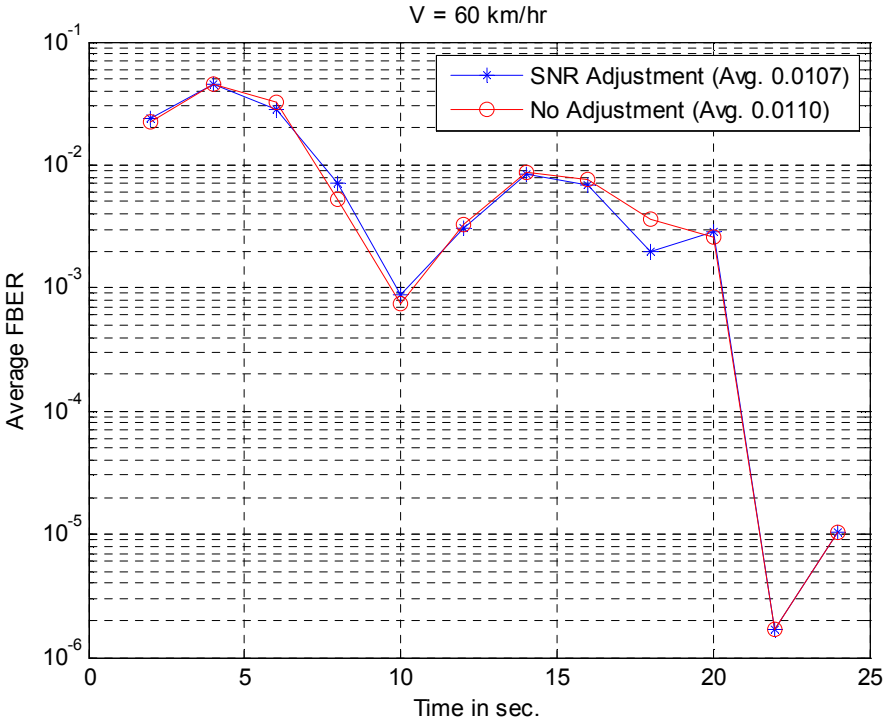

Fig. 4.5(b) Impact of SNR adjustment on the FBER with velocity 60 km/hr.

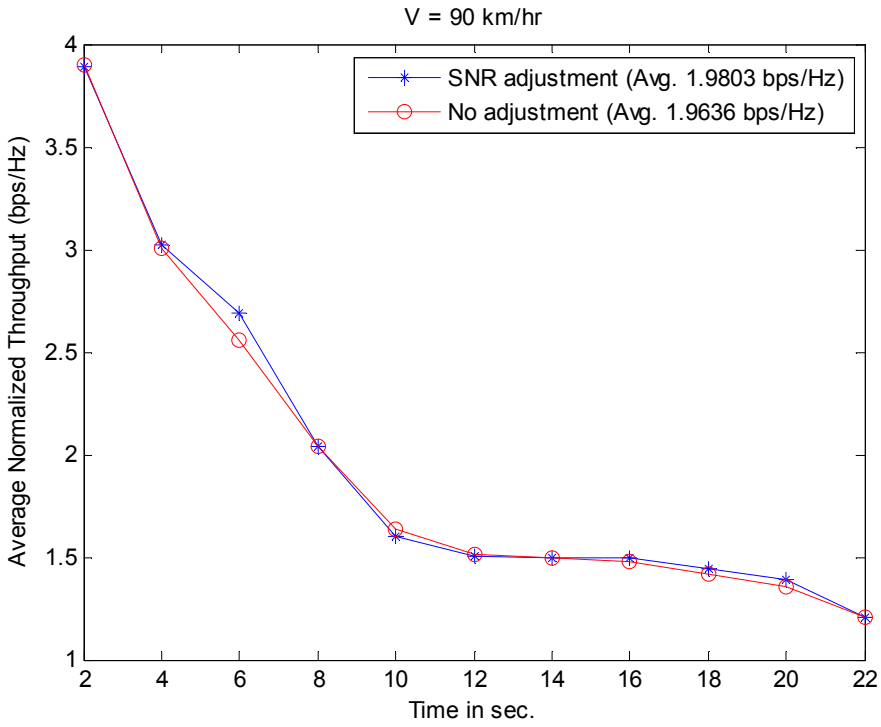

Fig. 4.6(a) Impact of SNR adjustment on the throughput with velocity 90 km/hr.

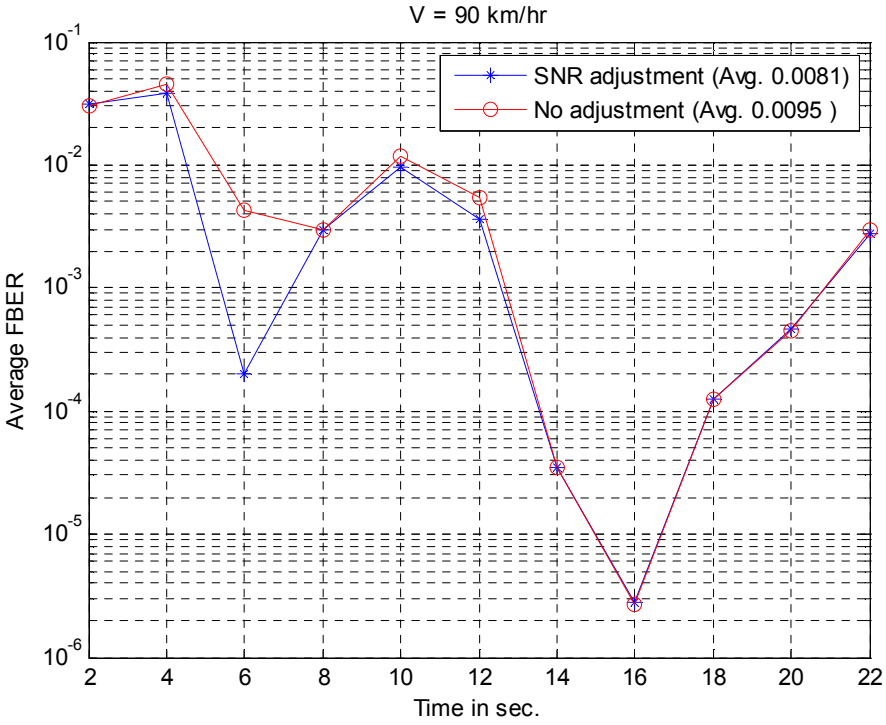

Fig. 4.6(b) Impact of SNR adjustment on the FBER with velocity 90 km/hr.

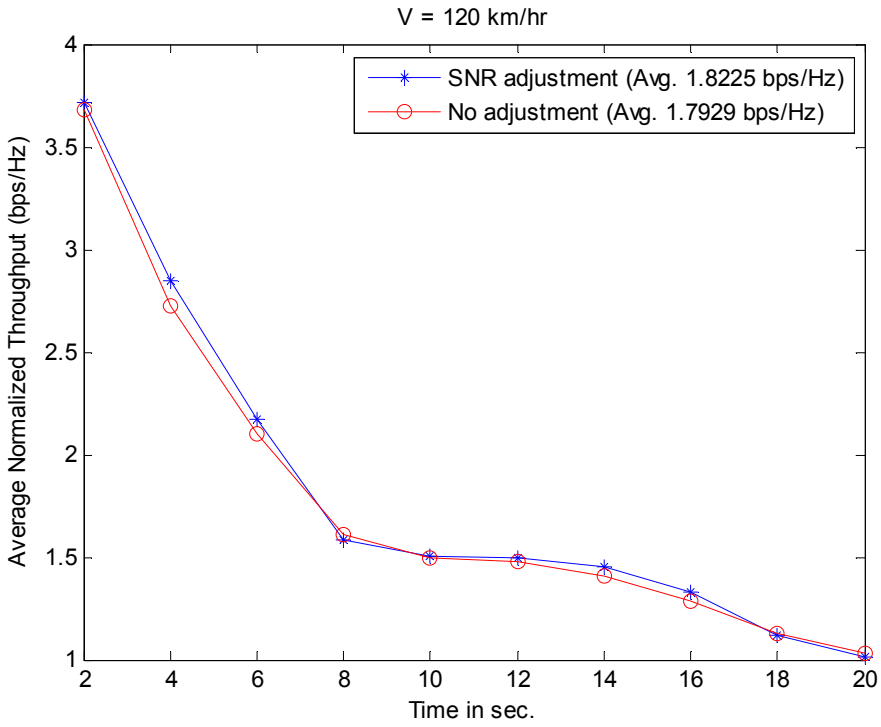

Fig. 4.7(a) Impact of the SNR adjustment on the throughput with velocity 120 km/hr.

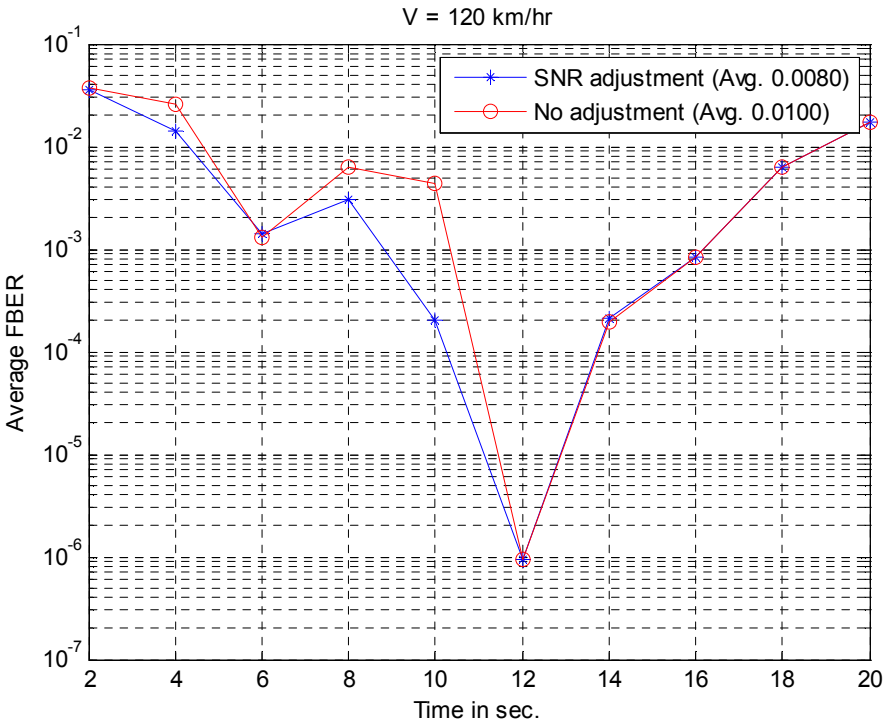

Fig. 4.7(b) Impact of SNR adjustment on the FBER with velocity 120 km/hr.

of the FBER is 0.0080 for the velocity based SNR adjustment, whereas that for the non-adjusted SNR is 0.0100.

According to the discussions above, we can conclude that the velocity based SNR adjustment improves overall performance. This improvement may come in the form of increased throughput or reduced FBER or both.

4.5 Impact of Adaptive ARQ

In section 2.6 of chapter 2, we mentioned that an adaptive ARQ mechanism is embedded in the proposed LA algorithm. This mechanism ensures more reliable transmission when it is required. The proposed adaptive ARQ mechanism selects a lower spectral efficiency burst profile if the previous frame is erroneously received (NACK message). Basically, it reduces FBER at the cost of spectral efficiency or throughput. Reduction of FBER also reduces the chance of data block dropping. It is well known that the truncated ARQ mechanism is widely used in wireless communications. We compare the performance of the proposed ARQ and that of the truncated ARQ for our devised mobile hotspot downlink.

We consider a departing mobile hotspot with a velocity of 90 km/hr. The initial distance is set to 200 meters from the BS. The allocated power is set to 0.5 Watt (27 dBm). The maximum number of retransmissions is set to 3 in both cases. Therefore, a frame must be successfully received within 4 successive trials to avoid dropping. Numerical results are obtained for 25 seconds duration (5000 frames). We take the average of every 1 sec interval.

Fig. 4.8(a) and Fig. 4.8(b) show the comparative average normalized throughput plots and the comparative average FBER plots, respectively. We see that the proposed adaptive ARQ provides lower throughput but lower FBER compared to the truncated ARQ. Overall average of the normalized throughput is 1.8873 bps/Hz for the proposed adaptive ARQ, whereas that for the truncated ARQ is 1.9045 bps/Hz.

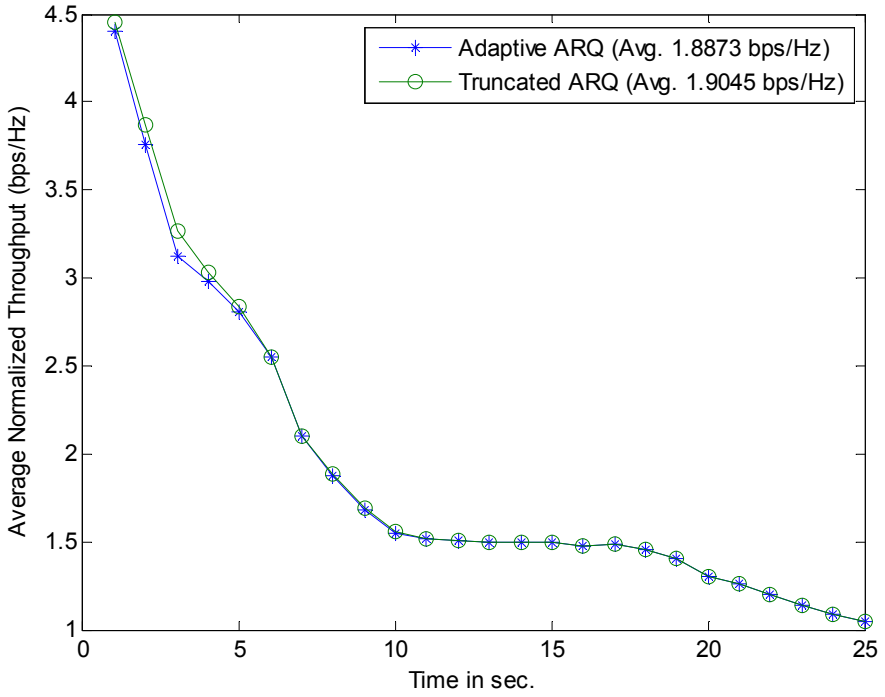

Fig. 4.8(a) Throughput comparison between adaptive ARQ and truncated ARQ.

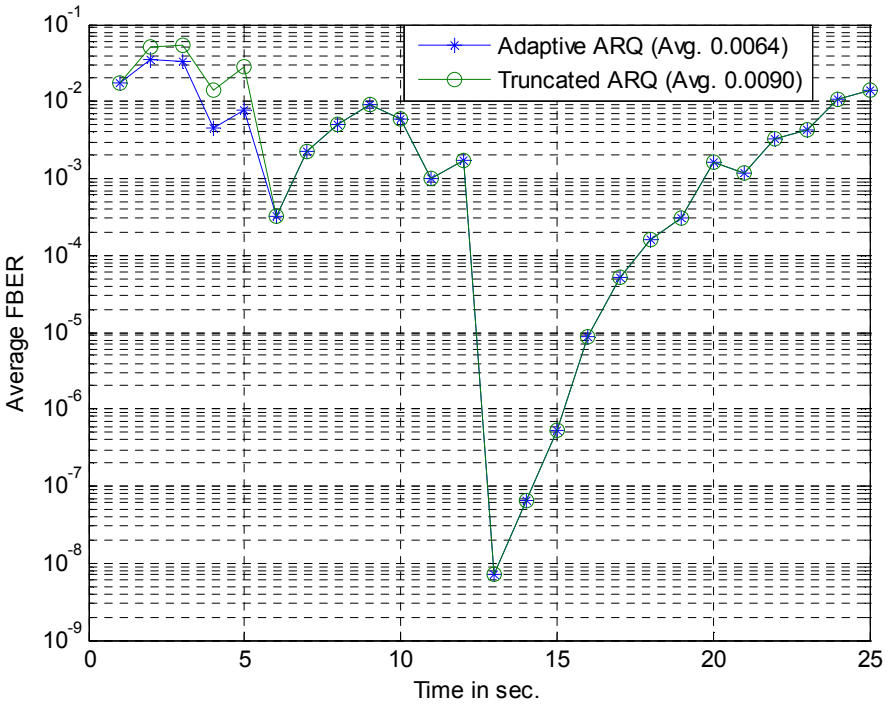

Fig. 4.8(b) FBER comparison between adaptive ARQ and truncated ARQ.

Overall average of the FBER is 0.0064 for the proposed truncated ARQ, whereas that for the truncated ARQ is 0.0090. It is observed that the proposed adaptive ARQ reduces normalized throughput by 0.9% but reduces FBER by 29%.

We obtain some other statistics which are not traceable from the plots of Fig. 4.8(a) and Fig. 4.8(b), but are important to know. There are 45 (0.9%) NACK frames observed for the proposed adaptive ARQ, whereas the number is 63 (1.26%) for the truncated ARQ. Moreover, there is no dropping event observed for the proposed adaptive ARQ. It means there is no 4 successive transmission failures occurred during 25 seconds. However, there are 2 dropping events observed for the truncated ARQ during 25 seconds. The proposed adaptive ARQ reduces chance of successive transmission failure.

According to the discussions above, we can conclude that the proposed adaptive ARQ fulfills our objective.

4.6 Summary

Throughput is dominated by path loss; moving direction is a key factor for throughput versus time characteristics. In most of the cases, the proposed LA algorithm is able to keep FBER under a certain value. Throughput reduces in higher departing velocities and increases in higher arriving velocities. FBER does not maintain any regular relationship with velocity. Velocity based SNR adjustment improves performance in both ways: increases throughput and reduces FBER. The proposed adaptive ARQ mechanism is able to reduce FBER at the cost of throughput. As a result number of dropping event reduces.

Chapter 5

Conclusion and Future Work

5.1 Conclusion

In this thesis, we have proposed a simple LA algorithm for the WiMAX supported mobile hotspots. The algorithm is designed for the downlink part between the WiMAX BS and mobile hotspot AP. It is an instantaneous SNR based LA algorithm. LA is done on a frame by frame basis. The link level performance of the proposed algorithm has also been evaluated. We summarize the contributions from this thesis as follows:

- The proposed LA algorithm is independent of the RA techniques. An RA technique may allocate power among the subchannels without having knowledge on the LA algorithm. The allocated power may vary from frame to frame. The proposed LA algorithm is able to work with frame by frame power variation.

- The proposed LA algorithm requires only two types of information: information on channel response and ACK/NACK message status of each frame. As per IEEE 802.16e standard, it is mandatory for the mobile WiMAX BS to record and update these information frame by frame basis. Therefore, there is no additional load on the network.

- We have not only proposed an LA algorithm but also proposed a simple channel estimation technique for the mobile WiMAX downlink. The proposed LA algorithm is also compatible with any other channel estimation technique.

- The proposed LA algorithm includes an intra subchannel power allocation strategy, velocity based SNR adjustment, and an adaptive ARQ mechanism. The advantages of these features are verified from the numerical results.

- The proposed LA algorithm is able to work under various types of conditions. It is adaptive with velocity, power, direction, channel response, and system performance.

- Though the proposed LA algorithm is for the mobile WiMAX networks, it can be extended to any other MIMO-OFDMA networks.

5.2 Future Work

Future research on LA for mobile hotspot can be extended to many other aspects as follows.

- The proposed LA algorithm can be extended to the multiuser cases. Two types of multiuser case can be considered: (i) homogeneous (a number of simultaneous mobile hotspots under the same BS, and (ii) heterogeneous (mobile hotspots, and pedestrian users simultaneously under the same BS).

- Efficient spectrum usage and power efficient algorithm design are two everlasting research issues for any OFDMA systems. A combined RA and LA framework can be developed for WiMAX supported mobile hotspot. It will make the network more efficient in both ways spectrum efficient and power efficient.

- High velocity mobile hotspot requires frequent handoff. The Mobile WiMAX supports some advanced handoff features such as FBSS and MDHO. A cross layer LA technique can be developed considering the handoff features of mobile WiMAX. A resource reservation based RA techniques can also be developed considering these handoff features.

- Application aware LA techniques can be developed for mobile hotspots. It will add a new dimension to LA.

- Performance improvement of the proposed LA algorithm can be achieved from modification of threshold table for the SM mode, and modification of SNR adjustment factor.

APPENDIX I

Post-Detection SNR for the SM mode with ZF detection

In case of a 2×2 MIMO configuration, the channel matrix B for subcarrier n,

$$\mathbf{H}(n) = \begin{bmatrix} h_{11}(n) & h_{12}(n) \\ h_{21}(n) & h_{22}(n) \end{bmatrix} \tag{A.I.1}$$

Pseudo inverse and inverse are the same in case of square matrices i.e. where $N_t = N_r$

$$\mathbf{G}(n) = \mathbf{H}(n)^{-1} = \begin{bmatrix} \dfrac{h_{22}(n)}{h_{11}(n)h_{22}(n) - h_{12}(n)h_{21}(n)} & \dfrac{-h_{12}(n)}{h_{11}(n)h_{22}(n) - h_{12}(n)h_{21}(n)} \\ \dfrac{-h_{21}(n)}{h_{11}(n)h_{22}(n) - h_{12}(n)h_{21}(n)} & \dfrac{h_{11}(n)}{h_{11}(n)h_{22}(n) - h_{12}(n)h_{21}(n)} \end{bmatrix}$$

$$= \frac{1}{\Delta}\begin{bmatrix} h_{22}(n) & -h_{12}(n) \\ -h_{21}(n) & h_{11}(n) \end{bmatrix} \tag{A.I.2}$$

where $\Delta = \mathbf{det(H}(n)\mathbf{)} = h_{11}(n)h_{22}(n) - h_{12}(n)h_{21}(n)$, we may drop subcarrier index for convenience.

$$[\mathbf{GG^H}] = \frac{1}{|\Delta|^2}\begin{bmatrix} |h_{22}|^2 + |h_{12}|^2 & -h_{11}^{*}h_{12} - h_{21}^{*}h_{22} \\ -h_{11}h_{12}^{*} - h_{21}h_{22}^{*} & |h_{11}|^2 + |h_{21}|^2 \end{bmatrix} \tag{A.I.3}$$

In the SM mode two symbols are transmitted simultaneously using two different antennas. Allocated power to a subcarrier is divided by two, SNR for the 1st symbol and 2nd symbol can be written as,

$$\Gamma_1 = \frac{s|\Delta|^2}{2\sigma^2(|h_{22}|^2 + |h_{12}|^2)} \text{ and } \Gamma_2 = \frac{s|\Delta|^2}{2\sigma^2(|h_{11}|^2 + |h_{21}|^2)}$$

We should consider both antennas (i.e. all the spatial channels) in order to set a threshold value. Taking a simple average of the denominators, we obtain an interesting expression for post-detection SNR for the SM mode with ZF detection

$$\Gamma_{SM} = \frac{s|\Delta|^2}{\sigma^2(|h_{22}|^2 + |h_{12}|^2 + |h_{11}|^2 + |h_{21}|^2)} = \frac{s|\Delta|^2}{\sigma^2 \|\mathbf{H}\|_{\mathbf{F}}^2} \quad \text{(A.I.4)}$$

APPENDIX II

Selection of Adjustment Factor (α)

We introduce the parameter α is to include the impact of mobility in SNR estimation. We define α as the ratio of minimum coherence time to current coherence time:

$$\alpha := \frac{T_{c,\min}}{T_{c,current}} \tag{A.II.1}$$

where $T_{c,\min}$ is the minimum coherence time which is related to the maximum Doppler shift or the maximum velocity of a mobile hotspot.
$T_{c,current}$ is the current coherence time which is related to the current Doppler shift or the current velocity of a mobile hotspot.

We know that coherence times are inversely proportional to the corresponding Doppler shifts, it means $T_{c,\min} \propto \frac{1}{f_{D,\max}}$ and $T_{c,current} \propto \frac{1}{f_{D,current}}$. The equation (A.II.1) turns into,

$$\alpha = \frac{f_{D,current}}{f_{D,\max}} = \frac{v_{current}}{v_{\max}} \tag{A.II.2}$$

where $v_{current}$ and $v_{\max}$ are the current velocity and the maximum velocity of a mobile hotspot respectively. The BS can get the exact value of the current velocity from mobile hotspot.

The upper bound of $v_{\max}$ can be obtained as follows:

maximum Doppler shift < subcarrier spacing

(This condition avoids the impact of Doppler's effect.)

or, $\frac{v_{\max} f_c}{c} < \Delta f$

or, $v_{\max} < \frac{c\Delta f}{f_c}$ (A.II.3)

This upper bound is very loose because signal power does not confine within the centre frequency. We define a spreading margin, which is the difference between subcarrier spacing and subcarrier bandwidth (BW_{SC}) as shown in Fig. A.II. It will help us to ignore intercarrier interference (ICI). Spreading margin is the maximum tolerable frequency spreading without any overlapping between two successive subcarriers. In our system $\Delta f = 10.94$ kHz and $BW_{SC} = 9.76$ kHz.

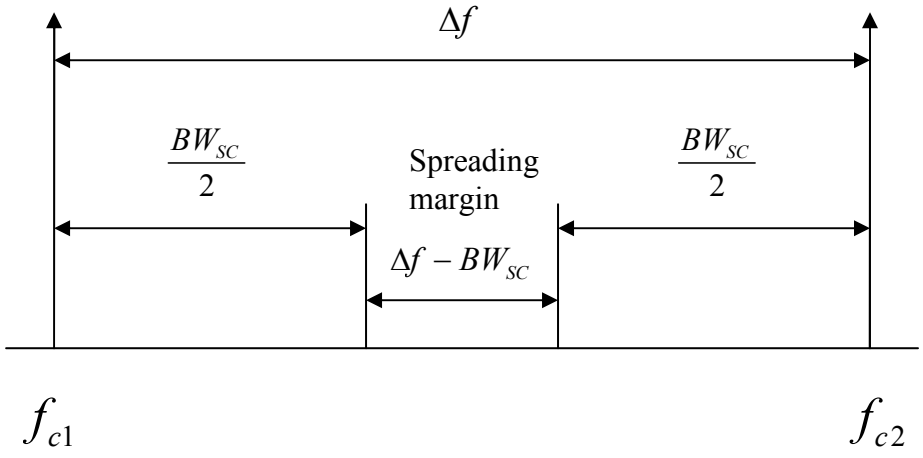

Fig. A.II: Spreading margin

We use spreading margin to find upper bound of $v_{\max}$ as follows,

$$v_{\max} < \frac{c}{f_c}\left(\Delta f - BW_{SC}\right)$$

$$v_{\max} < 554 \quad \text{km/hr}$$

We choose 360 km/hr as $v_{\max}$, we left some portion for frequency offset effect. Frequency spread occurs due to Doppler spread and subcarrier (carrier) frequency offset effect [39]. In reality, the mobile hotspot will never be operated with velocity $v_{\max}$. We define $v_{\max}$ as the velocity, at which channel estimation does not work at all. In other words, the channel is totally untraceable at $v_{\max}$.

Bibliography

[1] IEEE 802.16e-2005 and IEEE 802.16-2004/Cor 1-2005 (Amendment and Corrigendum to IEEE Std 802.16-2004), "IEEE Standard for Local and Metropolitan Area Networks Part 16: Air Interface for Fixed and Mobile Broadband Wireless Access Systems Amendment 2: Physical and Medium Access Control Layers for Combined Fixed and Mobile Operation in Licensed Bands and Corrigendum 1," 2006.

[2] S. Pack, H. Rutagemwa, X. Shen, J. W. Mark and L. Cai, "Performance Analysis of Mobile Hotspots with Heterogeneous Wireless Links," IEEE Trans. on Wireless Comm. Vol. 6, No. 10, pp. 3317-3726, Jan. 2007.

[3] S. Pack, X. Shen, J. W. Mark and L. Cai, "Throughput Analysis of TCP-friendly Rate Control in Mobile Hotspots," IEEE Trans. on Wireless Comm. Vol. 7, No. 1, pp. 193-203, Jan. 2008.

[4] D. Ho and S. Valaee, "Information Raining and Optimal Link-Layer Design for Mobile Hotspots," IEEE Trans. on Mobile Computing, Vo. 4, No.3, pp. 271-284, May/June 2005.

[5] V. Schena, F. Ceprani, "FIFTH project Solutions New Satellite Broadband Communication System for High Speed Train," Proceedings of VTC Spring 2004, Milan, Italy, May, 2004, pp.2831-2835.

[6] G. Sciascia et al "Statistical Characterization of the Railroad Satellite channel at Ku-Band" International Workshop of COST Actions 272 and 280 Noordwijk, Netherlands, May, 2003.

[7] A. Iera et al "Gateway Discovery and Selection in Mobile Hotspot," Proceedings of Auswireless 2006, Sydney, Australia, March 2006.

[8] A. Y. T. Chung, M. Hassan, "Traffic distribution schemes for multi-homed mobile hotspots," Proceedings of VTC Spring 2005, Stockholm, Sweden, May 2005, pp. 2127 – 2131.

[9] WiMAX Forum “Mobile WiMAX Part I: A Technical Overview and Performance Evaluation,” August 2006.

[10] H. Yagoobi, “Scalable OFDMA Physical Layer in IEEE 802.16 WirelessMAN”, Intel Technology Journal, Vol. 08, Issue 3, pp. 201-212, August 2004.

[11] V. Deverapalli et al, “NEMO basic support protocol” IETF RFC 3963 Jan.2005.

[12] L. Nuaymi, **WiMAX: Technology for Broadband Wireless Access**, John Wiley & Sons, 2007.

[13] R W Heath, A. J. Paulraj, “Switching Between Diversity and Multiplexing in MIMO Systems,” IEEE Trans. on Comm. Vol. 53, No. 6, pp. 962-968, June 2005.

[14] K. Balachandran et al, “Design and Analysis of an IEEE 802.16e based OFDMA Comm. System” Bell Lab. Tech. Journal 11(4), pp. 53-73, 2007.

[15] J. G. Andrews, A. Ghosh, and R. Muhamed, **Fundamentals of WiMAX**, Prentice Hall publishers 2007.

[16] B. Muquet, E. Biglieri, A. Goldsmith, and H. Sari, "An Analysis of MIMO Techniques for Mobile WiMAX Systems," chapter 1 in Advances in Mobile WiMAX, pp. 1-16, Editor: K.C. Chen, John Wiley & Sons, 2007.

[17] S. M. Alamouti, “A Simple Transmit Diversity Technique for Wireless Communications,” IEEE Trans. on Selected Areas in Comm., Vol. 16, No. 8, pp. 1451-1458, OCT. 1998.

[18] Q. Liu, S. Zhou, and G. B. Giannakis, “Cross-Layer Combining of Adaptive Modulation and Coding with Truncated ARQ over Wireless Links,” IEEE Transactions on Wireless Communications, Vol. 3, No. 5, pp. 1746-1755, Sept. 2004.

[19] IEEE “IEEE Standard for Local and Metropolitan Area Network- Part 16: Air Interface for Fixed Broadband Wireless Access Systems,” IEEE 802.16-2004, June 2004.

[20] J. G. Proakis, **Digital Communications**, McGraw-Hill, 4th edition, 2000, New York.

[21] A. Goldsmith, **Wireless Communications**, Cambridge University Press, 2005.

[22] S. T. Chung, A.J. Goldsmith “Degrees of freedom in Adaptive Modulation: A Unified View,” IEEE Trans. on Comm. Vol. 49, Sept. 2001.

[23] A. Paulraj, R. Nabar, and D. Gore, **Introduction to Space-Time Wireless Communications**, Cambridge University Press, 2003.

[24] C. Chen, and L. Wang, "On the Performance of the Zero-Forcing Receiver Operating in the Multiuser MIMO System with Reduced Noise Enhancement Effect," IEEE Globecom, 3: 1294–1298, St. Louis, MO, December 2005.

[25] T. Kim and J. G. Andrews. Optimal pilot-to-data power ratio for MIMO-OFDM. In Proceedings, IEEE Globecom, 3: 1481–1485, St. Louis, MO, December 2005.

[26] J. W. Mark, and W. Zhuang, **Wireless Communications and Networking**, Prentice Hall, 1st edition, 2003, New Jersey.

[27] M. R. Raghavendra et al, "Parametric Channel Estimation for Pseudo-Random Tile-Allocation in Uplink OFDMA," IEEE Trans. on Signal Processing, Vol. 55, No. 11, Nov. 2007, pp. 5370-5381.

[28] K. Naoki ,Y. Wataru, S. Akio, M. Daisuke, and U. Shuta,"Measurement of demmel condition number for 2x2 MIMO-OFDM broadband channels," Vehicular Technology Conference, 2004. IEEE 59th,VTC 2004-Spring. 2004, pp. 294-298.

[29] www.mathworks.com

[30] B. Marquet, E. Biglieri, and H. Sari, "MIMO Link Adaptation in Mobile WiMAX Systems," IEEE WCNC 2007, March 2007, Hong Kong, pp. 1810-1813.

[31] D. Marabissi, D. Tarchi, F. Genovese, and R. Fantacci, "Adaptive Modulation in Wireless OFDMA Systems with Finite State Modeling," Proc. of IEEE Globecom '07, Nov. 2007, Washington, DC, USA, pp.5210-5214.

[32] T. H. Chan, M. Hamdi, C. Y. Cheung, and M. Ma,"A Link Adaptation Algorithm in MIMO-based WiMAX systems," Journal of Communications, Academy publishers, Vol. 2, No. 5, August 2007, pp. 16-24.

[33] M. C. Jeruchim, P. Balaban, and K. S. Shanmugan, **Simulation of Communication Systems**, Kluwer Academic Publishers, 2nd edition 2002, New York.

[34] J. G. Proakis, and M. Salehi, **Contemporary Communication Systems Using MATLAB**, PWS Publishing Company, 1998, Boston.

[35] ITU-R Recommendation M.1225, "Guidelines for evaluation of radio transmission technologies for IMT-2000," 1997

[36] W. C. Jakes, Editor, **Microwave Mobile Communications**. New York: John Wiley & Sons Inc., February, 1975.

[37] B. Sklar, “Rayleigh Fading Channels in Mobile Digital Communication Systems part I: Characterization,” IEEE Communications Magazine, July 1997, pp. 90-100.
[38] R. H. Clarke, "A Statistical Theory of Mobile Radio Reception". Bell Systems Technical Journal 47 (6): 957–1000, July–August 1968.
[39] J. Lee, H. Lou, D. Toumpakaris, and J. M. Cioffi, "Effect of carrier frequency offset on OFDM systems for multipath fading channels," IEEE GLOBECOM 2004, Volume 6, Date: 29 Nov.-3 Dec. 2004, Pages: 3721-3725 Vol. 6.